



1 **NO<sub>2</sub> and HCHO measurements in Korea from 2012 to 2016 from Pandora Spectrometer Instruments**  
2 **compared with OMI retrievals and with aircraft measurements during the KORUS-AQ campaign**  
3 **Jay Herman<sup>1</sup>, Elena Spinei<sup>2</sup>, Alan Fried<sup>3</sup>, Jhoon Kim<sup>4</sup>, Jae Kim<sup>5</sup>, Woogyung Kim<sup>3</sup>, Alexander Cede<sup>6</sup>, Nader**  
4 **Abuhassan<sup>1</sup>, Michal Segal-Rozenhaimer<sup>7,8</sup>**

5

6

7

8

9

10

11

12

13

14

15

16

17

18 **Correspondence email: [jay.r.herman@nasa.gov](mailto:jay.r.herman@nasa.gov)**

19 <sup>1</sup>**University of Maryland Baltimore County JCET**

20 <sup>2</sup>**Virginia Polytechnic Institute and State University, Blacksburg, VA 24061, USA**

21 <sup>3</sup>**Institute of Arctic & Alpine Research, University of Colorado, Boulder, Colorado**

22 <sup>4</sup>**Dept. of Atmospheric Sciences, Yonsei University, Seoul Korea**

23 <sup>5</sup>**Department of Atmospheric Science, Pusan University, Busan, Korea**

24 <sup>6</sup>**Goddard Earth Sciences Technology & Research (GESTAR) Columbia, Columbia, MD 21046, USA**

25 <sup>7</sup>**Earth Science Division, NASA Ames, Mountain View, California**

26 <sup>8</sup>**Bay Area Environmental Research Institute, Petaluma, California**

27

28



29 **NO<sub>2</sub> and HCHO measurements in Korea from 2012 to 2016 from Pandora Spectrometer Instruments**  
30 **compared with OMI retrievals and with aircraft measurements during the KORUS-AQ campaign**

31

32 **Abstract**

33

34 Nine Pandora Spectrometer Instruments (PSI) were installed at 8 sites in South Korea as part of  
35 the KORUS-AQ (Korea U.S.-Air Quality) field study integrating information from ground, aircraft,  
36 and satellite measurements for air-quality studies. The PSI made direct-sun measurements of  
37 total vertical column NO<sub>2</sub>, C(NO<sub>2</sub>), with high precision (0.05 DU, where 1DU = 2.69x10<sup>16</sup>  
38 molecules/cm<sup>2</sup>) and accuracy (0.1 DU) that were retrieved using spectral fitting techniques.  
39 Retrieval of Formaldehyde (HCHO) total column amounts were also obtained at five sites using  
40 the recently improved PSI. The retrievals have with high precision, but possibly lower accuracy  
41 than for NO<sub>2</sub> because of uncertainty about the optimum spectral window for all ground-based  
42 and satellite instruments. PSI direct-sun retrieved values of C(NO<sub>2</sub>) and C(HCHO) are always  
43 significantly larger than OMI retrieved C(NO<sub>2</sub>) and C(HCHO) for the OMI overpass times (13.5 ±  
44 0.5 hours). In urban areas, PSI C(NO<sub>2</sub>) averages are at least a factor of two larger than OMI  
45 averages. Similar differences are seen for C(HCHO) in Seoul and nearby surrounding areas. Late  
46 afternoon values of C(HCHO) measured by PSI are even larger, implying that OMI early  
47 afternoon measurements underestimate the effect of poor air quality on human health. The  
48 primary cause of the OMI underestimate is the large OMI field of view FOV that includes  
49 regions containing low values of pollutants. In relatively clean areas, PSI and OMI are more  
50 closely in agreement. C(HCHO) amounts were obtained for five sites, Yonsei University in Seoul,  
51 Olympic Park, Taehwa Mtn., Amnyeondo, and Yeosu. Of these the largest amounts of C(HCHO)  
52 were observed at Olympic Park and Taehwa Mountain, surrounded by significant amounts of  
53 vegetation. Comparisons of PSI C(HCHO) results were made with the Compact Atmospheric  
54 Multispecies Spectrometer CAMS during overflights on the DC-8 aircraft for Taehwa Mtn and  
55 Olympic Park. In all cases, PSI measured substantially more C(HCHO) than obtained from  
56 integrating the CAMS altitude profiles. PSI C(HCHO) at Yonsei University in Seoul frequently  
57 reached 0.6 DU and occasionally exceeded 1.5DU. The semi-rural site, Mt. Taehwa, frequently  
58 reached 0.9 DU and occasionally exceeded 1.5DU. Even at the cleanest site, Amnyeondo, HCHO  
59 occasionally exceeded 1 DU.

60

61 Keywords: Pandora, KORUS-AQ, NO<sub>2</sub>, HCHO, Formaldehyde, Korea

62



## 63 1 Introduction

64 The purpose of this paper is to present the retrieved amounts of nitrogen dioxide and  
65 formaldehyde, NO<sub>2</sub> and HCHO, obtained from Pandora Spectrometer instruments (PSI) during the  
66 KORUS-AQ campaign (Korea US Air Quality: May – June 2016). A detailed analysis of the algorithms and  
67 uncertainties is discussed by Spinei et al., 2018. A network of nine PSI was installed in Korea as part of  
68 the KORUS-AQ campaign at 8 locations (Fig. 1 and Table 1). Five of the sites were selected to be “down-  
69 wind” from Seoul, an extremely NO<sub>2</sub> polluted area. The intent of the network was to integrate column  
70 density observations of NO<sub>2</sub> and HCHO into a multi-perspective framework of observations including  
71 ground-based, satellite, and airborne measurements of air quality. Viewing air quality through these  
72 multiple perspectives is important for connecting observations from future geostationary satellites to air  
73 quality networks such that conditions both at the surface and aloft can be better understood and  
74 represented across unmonitored areas. The data are especially important for computer models used for  
75 forecasts and decision making. Five of the KORUS-AQ PSI had recently improved optics that permitted  
76 retrieval of total vertical column formaldehyde (C(HCHO)). Part of the network was installed in April  
77 2015, a year before the start of the campaign. Three PSI continue to operate in Korea, one each, in  
78 Busan and Seoul since 2012, and one in Gwangju operating since April 2015.

79 Measurements of daytime total columns in Dobson Units, where 1 DU = 2.69 x 10<sup>16</sup>  
80 molecules/cm<sup>2</sup>, C(NO<sub>2</sub>), C(O<sub>3</sub>) and C(HCHO) are obtained every 80 seconds, which enables the PSI to  
81 show rapid short term (minutes to hours)  
82 variations in most locations with significant  
83 pollution (e.g., C(NO<sub>2</sub>) > 0.2 DU). PSI  
84 measurements of the visible and UV wavelengths  
85 are obtained separately (40 seconds each). A  
86 visible wavelength blocking filter, U340, reduces  
87 stray light for UV measurements.

88

Table 1 KORUS-AQ Locations (South to North)

| Locations    | Alt(m) | Latitude  | Longitude  |
|--------------|--------|-----------|------------|
| Gwangju      | 33     | 35.2260 N | 126.8430 W |
| Busan        | 228    | 35.2353 N | 129.0825 W |
| Anmyeondo    | 41     | 36.5380 N | 126.3300 W |
| Taehwa Mtn   | 160    | 37.3123 N | 127.3106 W |
| Yeosu-1 & 2  | 90     | 37.3385 N | 127.4895 W |
| Songchon     | 49     | 37.4100 N | 127.5600 W |
| Olympic Park | 26     | 37.5232 N | 127.1260 W |
| Seoul        | 181    | 37.5644 N | 126.9340 W |

89

90 Details on the Pandora spectrometer  
91 instrument can be found in Herman et al., (2009  
92 and 2015) as well as a NASA Pandora website  
93 <https://avdc.gsfc.nasa.gov/pub/DSCOVER/Pandora>



**Fig. 1** KORUS-AQ sites for 9 Pandora instruments at 8 sites.



94 [/Web\\_Pandora/index.html](#) and the data used are available from  
95 <https://avdc.gsfc.nasa.gov/pub/DSCOVER/Pandora/DATA/KORUS-AQ/>

96  
97 The PSI consists of a small Avantes low stray light spectrometer (280 – 525 nm with 0.6 nm  
98 spectral resolution with 4 times oversampling) connected to an optical head by a 400 micron single  
99 strand fiber optic cable. The spectrometer is temperature stabilized at 20°C (68°F) inside of a weather  
100 resistant container. The optical head consists of a collimator and lens giving rise to a 1.6° FOV (field of  
101 view) FWHM (Full Width Half Maximum) with light passing through two filter wheels containing  
102 diffusers, a UV340 filter (blocks visible light), neutral density filters, and an opaque position (dark  
103 current measurement). When the diffuser is used, the FOV is increased to over 2°. The optical head is  
104 connected to a small suntracker capable of accurately following the sun's center using software running  
105 on a small computer-data logger contained in a weatherproof outer box along with the spectrometer in  
106 a second inner temperature controlled box. The PSI is capable of obtaining C(NO<sub>2</sub>), C(HCHO) and C(O<sub>3</sub>)  
107 amounts sequentially over a period of 80 seconds including two dark current determinations. The  
108 integration time for NO<sub>2</sub> in bright sun is about 4 milli-seconds that is repeated and averaged for 20  
109 seconds (up to 4000 measurements) to obtain very high signal to noise ratios and very high precision  
110 (precision < 0.01 DU). Similar comments apply to C(O<sub>3</sub>), but not to C(HCHO), since formaldehyde  
111 absorption spectrum is mixed in with absorption from NO<sub>2</sub> and O<sub>3</sub>. This causes cross-correlation effects  
112 in the retrieval algorithm that make C(HCHO) retrievals sensitive to the selection of the wavelength  
113 range. The main source of noise in the measurement comes from the presence of clouds or haze in the  
114 FOV, which increases the exposure time and reduces the number of measurements in 20 seconds.  
115 Accuracy in the DOAS-type retrieval is obtained using careful measurements of the spectrometer's slit  
116 function, wavelength calibration, knowledge of atmospheric absorption cross sections, and the solar  
117 spectrum at the top of the atmosphere. Accuracy for C(NO<sub>2</sub>) has been estimated to be ±0.05 DU. A  
118 recent addition of anti-reflection coatings to the PSI optics has improved accuracy and precision by  
119 reducing the residuals associated with spectral fitting using trace gas absorption cross sections. The  
120 reduced residuals are necessary for the retrieval of formaldehyde and bromine oxide that absorb in  
121 spectral regions dominated by ozone and NO<sub>2</sub>.

122  
123 This paper discusses the distribution of C(NO<sub>2</sub>) and C(HCHO) over Korea at the sites where the  
124 PSI were located (Fig. 1). Section 2 shows the amounts of NO<sub>2</sub> observed by PSIs at the 8 KORUS-AQ  
125 sites. Section 3 discusses the diurnal variation of NO<sub>2</sub>. Section 4 looks at longer term changes in NO<sub>2</sub>  
126 obtained from PSIs that were deployed before the beginning of the KORUS-AQ campaign. Section 5  
127 evaluates the disagreement with OMI satellite C(NO<sub>2</sub>) retrievals (Kramer et al., 2008). Section 6  
128 compared PSI C(NO<sub>2</sub>) retrievals with the aircraft overpass retrievals from the 4STAR instrument (Segal-  
129 Rozenhaimer et al., 2014). Section 6 discusses retrievals of C(HCHO) amounts for five PSI sites, the  
130 diurnal variation of C(HCHO), and comparisons with the Compact Atmospheric Multispecies  
131 Spectrometer CAMS (Richter et al., 2015) from DC-8 aircraft overflights of 5 PSI sites.

132  
133  
134  
135



## 136 2.0 NO<sub>2</sub> during the KORUS-AQ Campaign (May – June 2016)

137

138 An example of NO<sub>2</sub> retrieval from two independently calibrated Pandoras that were initially  
139 located at the same site (Yeosu, Korea, 37.3385°N, 127.4895°W) are compared in Fig. 2a showing that  
140 the difference in C(NO<sub>2</sub>) amount is less than 0.05 DU even in the presence of thin afternoon clouds (Fig.  
141 2b) that decrease the measured solar irradiance by more than a factor of 2. Though Yeosu is a relatively  
142 clean site in Korea (located to the southeast of Seoul Lat=37.5644°N, Long=126.934°W), C(NO<sub>2</sub>) amounts  
143 frequently reach moderately high values (e.g., 1 DU on 3 June 2016), and occasionally even higher (2-3  
144 DU). However, Yeosu has much less C(NO<sub>2</sub>) compared to Seoul, less than 30 km distant, where PSI  
145 measurements were found to reach over 3 DU (Fig. 3) during the campaign period from mid-April to  
146 early June, 2016.

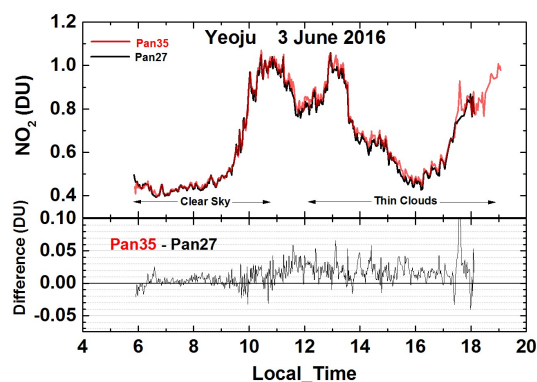


**Fig. 2a** C(NO<sub>2</sub>) amounts from Pandora 27 and 35 in Yeosu, Korea during 3 June 2016 and their difference (Pan35 – Pan27) < 0.05 DU. An estimate of the cloud cover effect on measured radiances (counts/second) is shown in Fig. 2b.

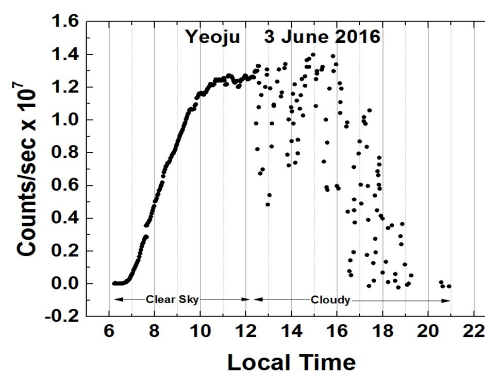


**Fig. 2b** Pandora 35 estimate of cloud or aerosol cover from measured counts/second at approximately 500 nm showing a near noon count rate of  $1.26 \times 10^7$  counts/second followed by a reduced count rate as clouds move in front of the sun. The cloud or aerosol cover estimate is from the same date 3 June 2016 as the C(NO<sub>2</sub>) amounts shown in Fig.2a.

147 In a manner similar to Fig. 2a, C(NO<sub>2</sub>) amounts can show large variability from day-to-day and  
148 intraday, as well as between different sites. The largest amounts of C(NO<sub>2</sub>) are in the north (Seoul and  
149 Olympic Park) associated with the largest population and industry concentrations, while the southern  
150 cities of Busan and Gwangju have smaller amounts of C(NO<sub>2</sub>). The smallest C(NO<sub>2</sub>) amounts are at  
151 Anmyeondo (an island on west coast of Korea 42 km south of Seoul, usually not downwind of Seoul),  
152 and Songchon to the east of Seoul.

153

154 Figure 2b shows the effect of thin clouds in terms of reduced measured count rates for a single  
155 spectrometer pixel near 500 nm. The effect of thin clouds for C(NO<sub>2</sub>) retrieval (Fig. 2a) is increased noise  
156 (reduced precision) with a very small impact on accuracy. There are two effects on PSI observations to  
157 consider in association with thin clouds. First, is multiple scattering within the cloud affecting the optical



158 path and effective air mass factor AMF. This has a very small effect on AMF, since most of the  $\text{NO}_2$  is  
 159 near the surface well below the clouds. Second, is the reduction in the number of measurements during  
 160 a fixed 20 second measuring period causing a decrease in the signal to noise ratio. The weather during  
 161 the campaign was occasionally very cloudy, which caused some missing  $\text{NO}_2$  and  $\text{O}_3$  data. However,  
 162 most of the cloudy days were light to moderate cloud cover, which permitted  $C(\text{NO}_2)$  amounts to be  
 163 determined, but with lower precision compared to clear-sky direct sun measurements (e.g., Fig.s 2a and  
 164 b). When the cloud cover becomes sufficiently thick, precision is reduced (increased point-to-point  
 165 scatter) and the spectral fitting error increases. A small percentage of data points with high retrieval  
 166 error,  $C(\text{NO}_2 \text{ Error}) > 0.1 \text{ DU}$ , have been removed from the data set.

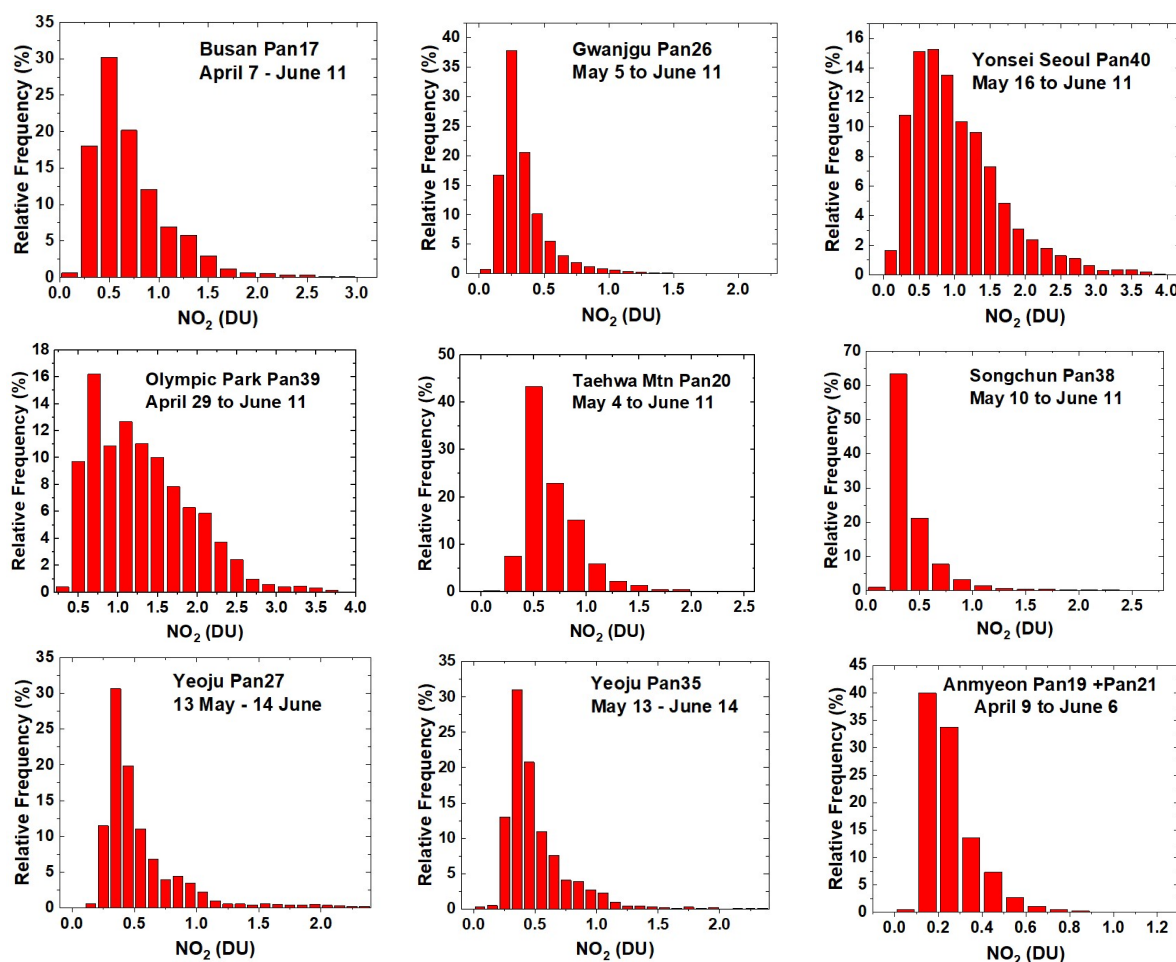


Fig. 3. Frequency distributions of  $C(\text{NO}_2)$  across the KORUS-AQ PSI network: April 20 to Jun 6 2016, except as labelled. The axes vary for different sites.



168 Figures 3 and 4 summarize all of the Pandora  $C(\text{NO}_2)$  data obtained during the KORUS-AQ  
169 campaign. Figure 3 presents histograms in percent frequency of occurrence for all nine sites. All of the  
170 sites located within or downwind of major cities have production of  $\text{NO}_x$  mainly from transportation and  
171 power generation as its major sources. The ratio of transportation  $\text{NO}_x$  production compared to all  
172 other sources is estimated as up to a factor of three (Kim et al., 2013).  
173

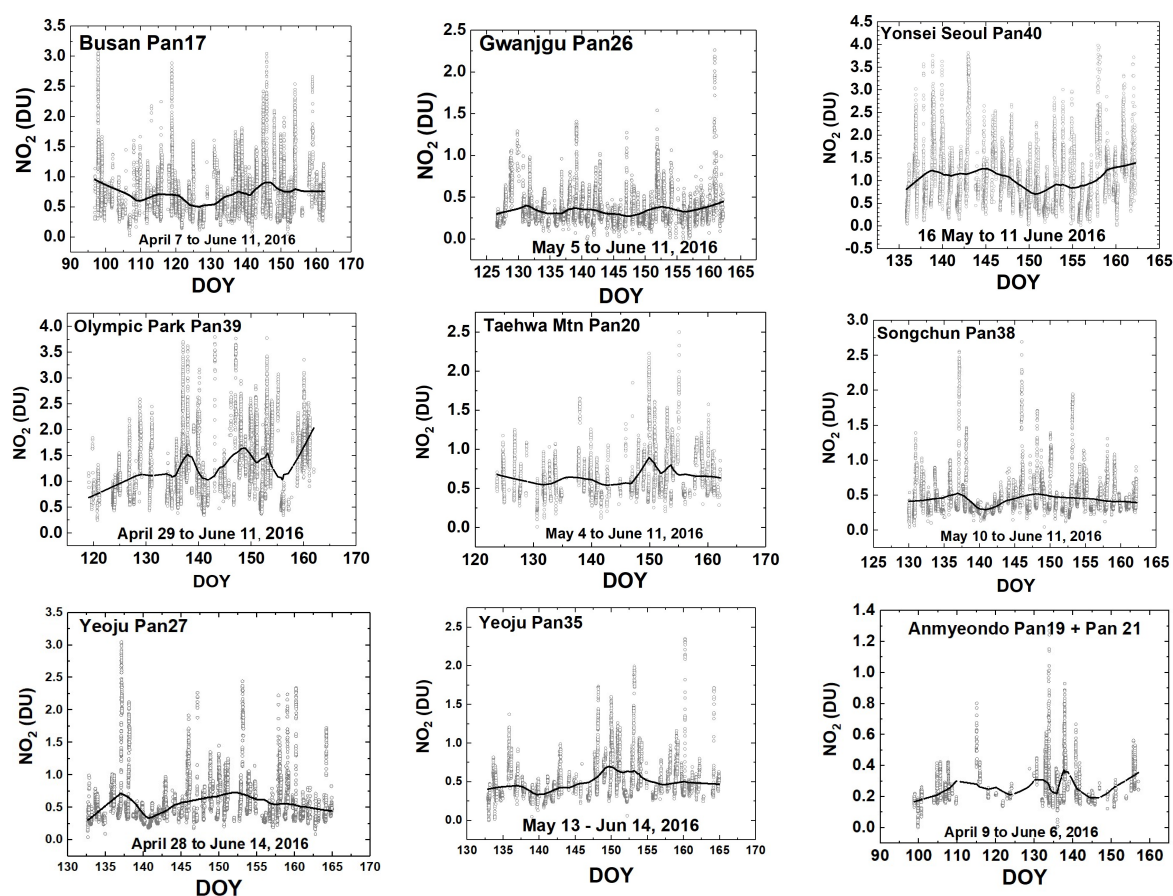


Fig. 4  $\text{NO}_2$  time series vs day of the year (DOY) and diurnal variability (daily vertical extent) at 9 Pandora sites. Notice the very high  $\text{NO}_2$  amounts in Seoul and nearby Olympic Park. The black curves are approximately weekly least squares running averages. The daily vertical extent corresponds to diurnal variation (Fig. 2). Note: the vertical scales are different for each site to show the daily variability relative to the running average.

174

175

176

177

178

179

The Seoul site frequently has amounts of  $C(\text{NO}_2)$  greater than 2 DU. The same is true of Olympic Park, located in the eastern part of the Seoul metropolitan area. For locations increasingly distant from Seoul, the amount of  $C(\text{NO}_2)$  decreases in response to smaller local emissions, since the short chemical lifetime of  $\text{NO}_2$  normally precludes long distance transport. Compared to Seoul, the two smaller southern cities, Gwangju and Busan, have relatively low levels of  $C(\text{NO}_2)$  on most days, with the most



180 typical values ranging from 0.3 to 0.5 DU, although high values exceeding 2 DU can occur on rare  
181 occasion.

182

183 Figure 4 shows the same data as Fig. 3, but in the form of a time series covering the KORUS-AQ  
184 period. The daily variation (at least one point every two minutes) is shown in the vertical extent  
185 corresponding to each day's data. Figures 3 and 4 are consistent with a large NO<sub>2</sub> pollution source in the  
186 Seoul metropolitan area that tends to transport eastward through nearby Olympic Park and gradually  
187 diluting by the time air masses reach Taehwa, Songchon, and Yeosu. Even though average C(NO<sub>2</sub>)  
188 amounts are much lower at Songchon and Yeosu, there are times when the pollution levels are quite  
189 high (C(NO<sub>2</sub>) > 2 DU, Fig. 5). There are days when the amount of C(NO<sub>2</sub>) gets close to 4 DU in Seoul, 3  
190 DU in Olympic Park and Busan, and 4 DU for one day in Yeosu (April 27). The southern cities, Busan and  
191 Gwangju are much less polluted on average, which results in a much smaller effect on adjacent regions.  
192 Busan is located on the southeastern coastline, so that much of its NO<sub>2</sub> pollution dissipates over the  
193 ocean, except for occasional days when very high amounts (3 DU) occur. Anmyeondo is quite clean,  
194 since it is located on the western coast well south of Seoul. The most frequently occurring C(NO<sub>2</sub>) value  
195 at Anmyeondo is 0.15 – 0.2 DU, which means that the measured NO<sub>2</sub> amount are mostly from the  
196 stratosphere with very little tropospheric or boundary layer NO<sub>2</sub>. There are occasional C(NO<sub>2</sub>) plumes  
197 from industrial activity to the north, and, perhaps, from China.

198

### 199 **3 Diurnal Variation of C(NO<sub>2</sub>)**

200

201 Grouping the diurnal variation together from multiple days (Fig. 5) reveals a pattern to NO<sub>2</sub>  
202 emissions and accumulation related to the main NO<sub>2</sub> emission sources (automobiles and power  
203 generation) for the 3 largest cities in Korea: Seoul (Pan40), Busan (Pan17), and Gwangju (Pan26). For  
204 Seoul, the amounts of C(NO<sub>2</sub>) during the morning (1 DU at 10:00) are much less than later in the  
205 afternoon (over 2 -3 DU at 16:00) on almost every day with values occasionally reaching as high as 6 DU.  
206 Even the relatively low morning values of C(NO<sub>2</sub>) represent a significant amount of pollution. The 6 DU  
207 C(NO<sub>2</sub>) amount in Seoul is unusual, but coincides with the peak values frequently occurring in the late  
208 afternoon. C(NO<sub>2</sub>) behavior at nearby Olympic Park to the east of Seoul is very similar to Yonsei  
209 University in the heart of Seoul, even though Olympic Park's traffic density is lower than Seoul. Olympic  
210 Park is close enough to the metropolitan Seoul area for the transport of NO<sub>2</sub> combined with local  
211 production from traffic to produce a very similar diurnal pattern. The moderately large city of Busan also  
212 has high values of NO<sub>2</sub>, occasionally reaching 3 DU in the afternoon. Busan has relatively low values of  
213 NO<sub>2</sub> in the morning, having peaks in the mid-afternoon and declining in the late afternoon. Gwangju,  
214 located in the southwest, is a smaller city with less pollution (peak values = 1.6 DU) and does not have as  
215 distinct an afternoon maximum.

216

217

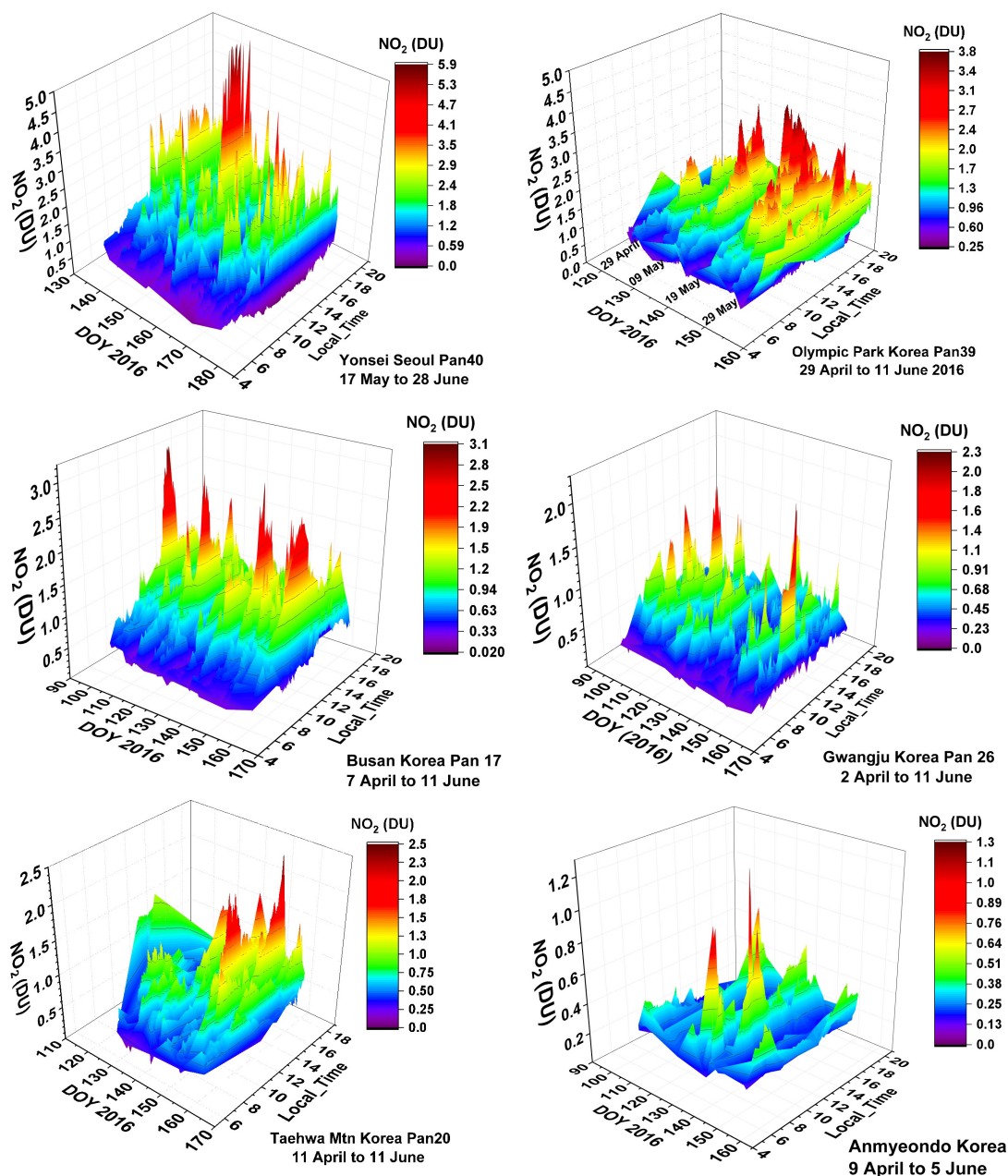


Fig. 5 NO<sub>2</sub> amounts vs Day of the Year (DOY) and Local Time for six sites as labeled in each panel. Day 120=April 29, Day 130=May 9, Day 140=May 19, Day 150=May 29, Day 160=June 8, Day 170 =June18.



219 The panels in Fig. 5 for Taehwa Mtn. and Anmyeondo show regions outside the Seoul  
220 metropolitan area that still show substantial amounts of NO<sub>2</sub>. Compared to Seoul, the Taehwa site is a  
221 semi-rural location with only a small amount of car traffic in the immediate area. However, there are  
222 major highways about 6 km from the site that are close enough to permit transport of NO<sub>2</sub> to the  
223 Taehwa Mountain site. All of the sites showed a tendency to have peak NO<sub>2</sub> occur in the late afternoon.  
224 Anmyeondo on the west central coast of Korea shows C(NO<sub>2</sub>) amounts that are quite low with  
225 occasional plumes arriving from the north or the west (China).

226 The basic daily pattern of C(NO<sub>2</sub>) in urban Korea arises from large amounts of automobile traffic  
227 and power plants emitting NO<sub>x</sub> (for modern automobiles, roughly 99 % NO and 1 % NO<sub>2</sub>). An FTIR  
228 analysis of automobile exhaust shows that NO is emitted at 127 ppm, NO<sub>2</sub> at 1.6 ppm, HCHO at 39 ppm,  
229 and CH<sub>3</sub>OH at 139 ppm as part of the main emissions containing H<sub>2</sub>O (143577 ppm) and CO<sub>2</sub> (122191  
230 ppm). (<https://tools.thermofisher.com/content/sfs/brochures/D10248~.pdf>).

231 NO quickly converts into NO<sub>2</sub> in the presence of ozone and volatile organic compounds VOCs in  
232 the atmosphere and can convert back to NO by solar photolysis. Model calculations (Boersma et al.,  
233 2009) and measurements in Israel show mid-day minima in NO<sub>2</sub>, which are different than the PSI  
234 observations in Korea showing increasing NO<sub>2</sub> throughout the day with peaks in the late afternoon. This  
235 implies that the amount of locally produced NO<sub>x</sub> and conversion into NO<sub>2</sub> dominates the losses of NO<sub>2</sub>  
236 by photolysis and transport out of the region.

#### 237 4.0 Longer-Term Changes in C(NO<sub>2</sub>)

238 Some of the sites used for the KORUS-AQ campaign (Gwangju and Anmyeondo) had PSIs set up  
239 in April 2015, about one year before the start of the campaign. Two other sites (Seoul and Busan) have  
240 PSI C(NO<sub>2</sub>) data starting in 2012. The extended data sets for Seoul and Busan provide the opportunity to  
241 estimate 5-year changes in C(NO<sub>2</sub>) amount and seasonal dependence.

242 In Fig. 6, the daily variation over one year at Gwangju and Anmyeondo are evaluated to estimate  
243 one year secular trends. The vertical extent in the time series is not noise or uncertainty, but rather the  
244 80 second per data point variability throughout each day (e.g., see Fig. 2). Before calculating linear least  
245 squares slopes, the unadjusted time series (Panels A and D) were deseasonalized (Panels B and E) by  
246 subtracting a function with zero slope derived from a 30 day running average (dark line in panels A and  
247 D). The running average curves in panels A and D are shown with expanded scale in panels C and F to  
248 show the seasonal variation. The “zero slope functions” are obtained by subtracting a linear least  
249 squares fit L(t) to monthly running average curves M(t) in panels C and F to form zero slope functions  
250 ZM(t) = M(t) – L(t). The results are functions that look similar to the plots in panels C and F, but with zero  
251 slopes. The resulting ZM(t) are then subtracted from the respective original time series (grey circles) in  
252 panels A and D. The results are the grey circles in Panels B and E. Similar monthly running means are  
253 shown in Panels B and E that have almost no monthly variations.

254 The linear trends in Figs. 6B and 6E suggest that there was an increase in pollution levels in  
255 Gwangju and Anmeondo over the period of observation. The southern city of Gwangju (Pan 26) has  
256 higher average C(NO<sub>2</sub>) amounts, 0.34±0.19 DU, compared to the relatively clean coastal site



257 Amnyeondo,  $0.26 \pm 0.14$  DU. Gwangju seasonal cycle has a minimum in C( $\text{NO}_2$ ) amount in September-  
 258 October and a very broad maximum from December to May. The Gwangju PSI is located away from  
 259 major city traffic on a university campus (Gwangju Institute of Science and Technology, GIST) so that the  
 260 average amount of  $\text{NO}_2$  (about 0.34 DU) is moderate with some days reaching 1.5 DU. The slopes are  
 261 statistically significant at the 2-standard deviation level ( $p < 0.05$ ) and imply that C( $\text{NO}_2$ ) was increasing  
 262 at a substantial rate. However, the period of observation was too short to estimate multi-year long-term  
 263 trends. Additional long-term monitoring of these sites would be desirable for air quality purposes.

264

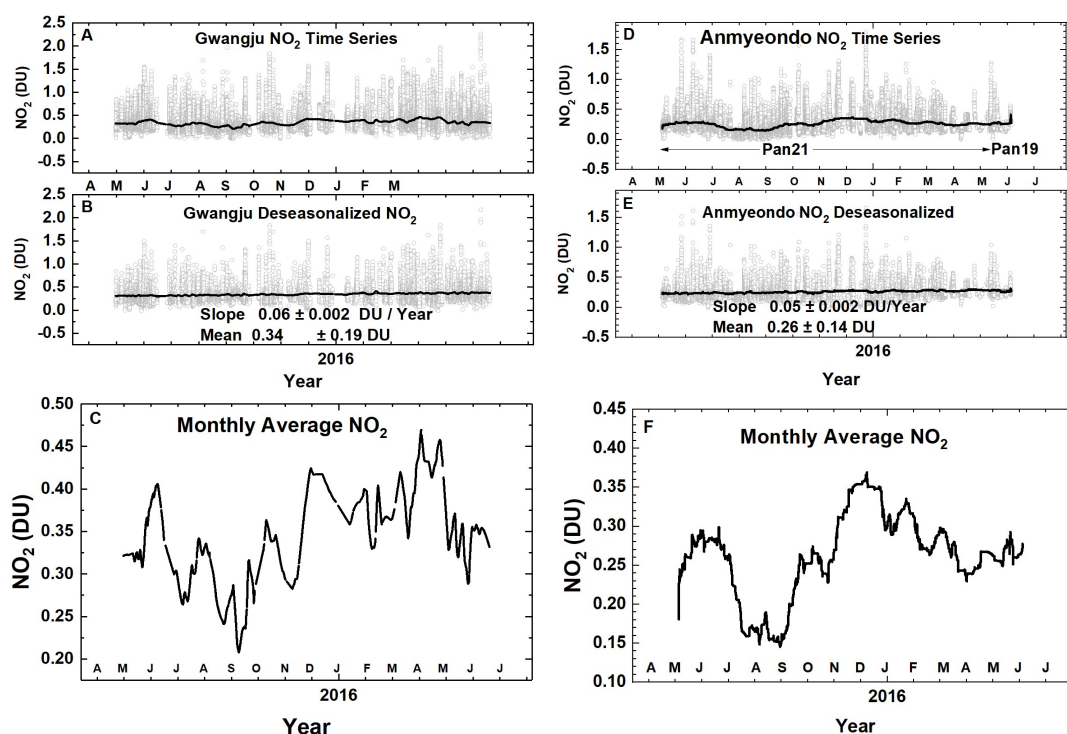


Fig. 6 Approximately 1 year of daily column C( $\text{NO}_2$ ) amount data, the monthly running average amount, and a linear least squares fit to the deseasonalized time series. The data are from GIST at Gwangju and Amnyeondo. Panels A and D are the original time series with one data point every 80 seconds, panels B and E are the deseasonalized time series and the trend in C( $\text{NO}_2$ ), and panels C and F are monthly running averages  $M(t)$  of C( $\text{NO}_2$ ) from the solid lines in panels A and D. The vertical extent (panels A, B, D, and E) on a given day is the range of diurnal variation from early morning to late afternoon.

265 The PSI on Amnyeondo was located away from a commercial area with moderate traffic and  
 266 very near the shore of the Yellow Sea at a regional Global Atmosphere Watch (GAW) station. For  
 267 Amnyeondo there is a clear seasonal cycle similar to that in Gwangju with a minimum in September-  
 268 October and a broad maximum during the winter-spring months. Amnyeondo had an average amount  
 269 of 0.25 DU, which is lower than observed at Gwangju.

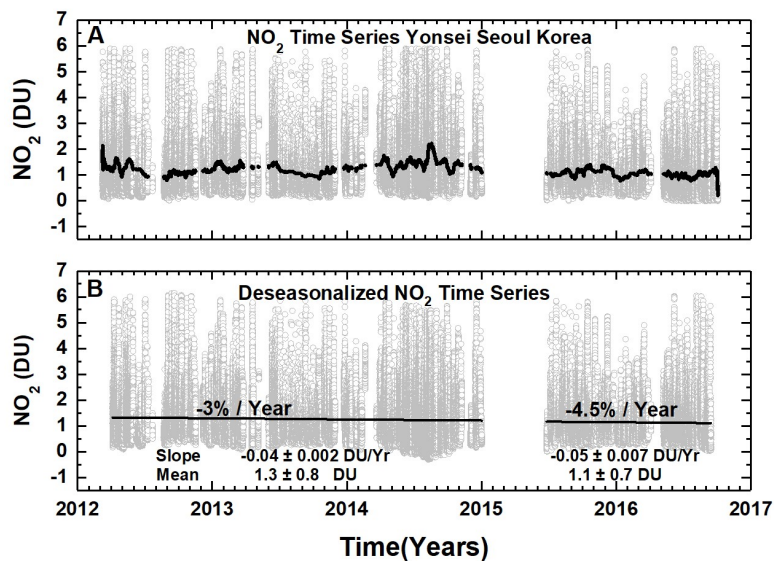


Fig. 7 (A)  $\text{NO}_2$  time series at Yonsei University in Seoul  $\text{NO}_2$ (grey) and (B) deseasonalized time series. Combined slope =  $-0.05 \pm 0.001 \text{ DU/Year}$  and Mean =  $1.2 \pm 0.8 \text{ DU}$  or the decrease is  $-4 \pm 0.08 \text{ \% / Year}$ . Seoul has no clear seasonal cycle.

270

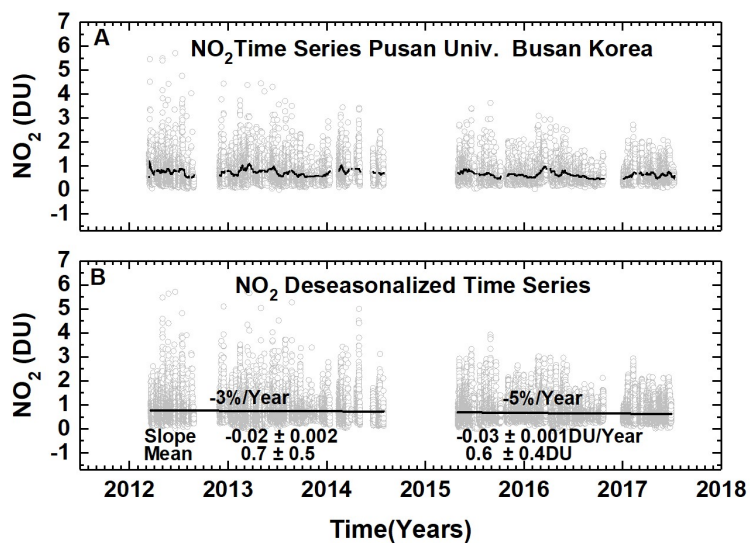


Fig. 8 (A) Pusan University in Busan  $\text{NO}_2$  daily time series (grey) and (B) deseasonalized time series with linear trends.

271



272            Figures 7 and 8 each contain an approximately 5-year daily time series (grey) for Seoul (Yonsei  
273 University) and Busan (Pusan University) and a linear fit to a deseasonalized version of the time series.  
274 Since the observations at both sites had an extended period of missing data, the slopes were estimated  
275 separately for each segment and for the combined time series. Both Seoul and Busan show a steady  
276 reduction in NO<sub>2</sub> air pollution with an average reduction of about -4 % per year. A recent paper by  
277 Duncan et al., (2016) estimated a decrease in C(NO<sub>2</sub>) for Seoul in about a 10 x 10 km box of about 1.6 ±  
278 1.4 % per year over the 2004 to 2013 period based on a 2014 average C(NO<sub>2</sub>) amount of 0.6 DU, or  
279 about half of the average value 1.3 ± 0.8 DU observed by the PSI. The larger reduction in C(NO<sub>2</sub>)  
280 measured by the PSI is caused by a reduction in higher than average afternoon C(NO<sub>2</sub>) amounts that are  
281 rarely observed by OMI overpass at 13:30 local time. The high observed late afternoon values are not  
282 restricted to Seoul, but occur for all of the urban areas where the PSI has been deployed. The high late  
283 afternoon values do not regularly occur in remote rural areas such as Amnyeondo.

284            Seoul and Busan C(NO<sub>2</sub>) measurements are remarkable for the large peak amounts that are seen  
285 on most days compared to the 1.5 to 2 DU peak values for Gwangju and Amnyeondo. For Yonsei, the  
286 peak values range above 5 to 6 DU in the years 2012 to 2015, but decrease somewhat in 2015 to 2016.  
287 In 2015 - 2016, the decrease appears to be large, but is only 0.2 DU relative to a mean of about 1.2 DU.  
288 A smaller decrease appears for Busan (Fig. 8) relative to a mean of about 0.6 DU. All of the PSI  
289 measurements show very high values of NO<sub>2</sub> during almost every day when measurements were  
290 possible. Since the NO<sub>2</sub> concentrations represented by these large column amounts are probably in the  
291 boundary layer near the sources of NO<sub>2</sub>, there is a strong effect on local air quality.

292

## 293 **5 Comparison with OMI Satellite Overpass Data**

294

295            Seoul and Busan have 5-year PSI data records (Figs. 9a and 9b), and Gwangju has a 1-year data  
296 record (Figs. 6 and 10) spanning the KORUS-AQ campaign. The PSI C(NO<sub>2</sub>) can be matched in time (± 8  
297 minutes) with the overpass time from OMI (Ozone Monitoring Instrument) onboard the AURA satellite  
298 (mid-day overpass times 13:30 ± 90 minutes). Figure 9a shows the C(NO<sub>2</sub>) daily variation at the OMI  
299 overpass time with far more high values of C(NO<sub>2</sub>) from the PSI than observed by OMI. The solid lines  
300 represent the seasonal dependence, which are shown separately in Fig. 9b along with the C(NO<sub>2</sub>)  
301 differences, PSI - OMI. The result is that the average PSI values are double those observed by OMI's  
302 large FOV. (OMI Version 03: <https://avdc.gsfc.nasa.gov/index.php?site=666843934&id=13>)

303

304            The seasonal dependence (Fig. 9b) of C(NO<sub>2</sub>) from OMI for both Seoul and Busan is fairly  
305 regular, with maxima in January of each year and minima in July-August. The seasonal behavior of  
306 C(NO<sub>2</sub>) obtained from the PSI for Seoul varies with high values extending from January into the summer  
307 months and with minima varying from August in 2012, September-October in 2013, missing in 2014, July  
308 in 2015, and June in 2016. For Busan, the maxima occur in the Spring for 2013 and 2014, October for  
309 2015, and in the Spring for 2016. The minima are also variable. The difference between OMI and PSI  
310 retrievals depends on local conditions for PSI and on an area average for OMI.

311



312

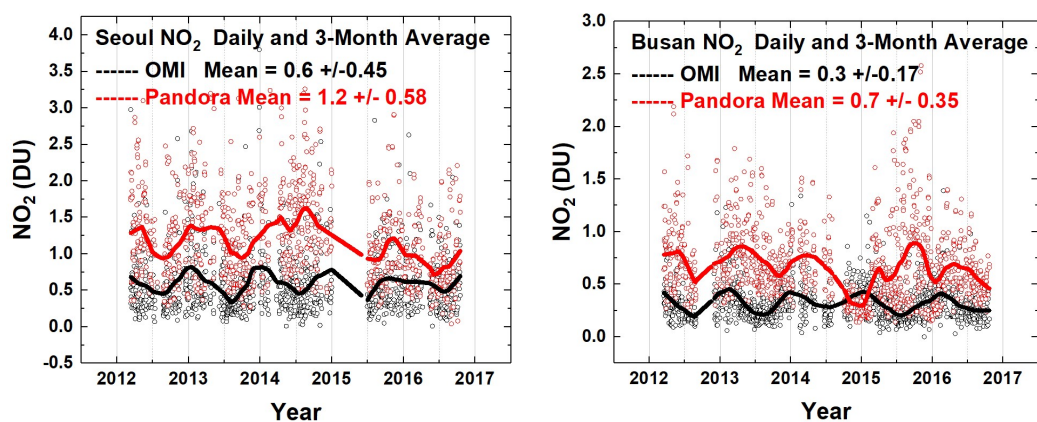


Fig. 9a Comparisons between the daily values of  $C(\text{NO}_2)$  for OMI (black) and PSI (red) at Seoul and Busan for a 5-year period. Solid lines show the average seasonal variation (Lowess(0.1)), see also Fig. 9b.

313

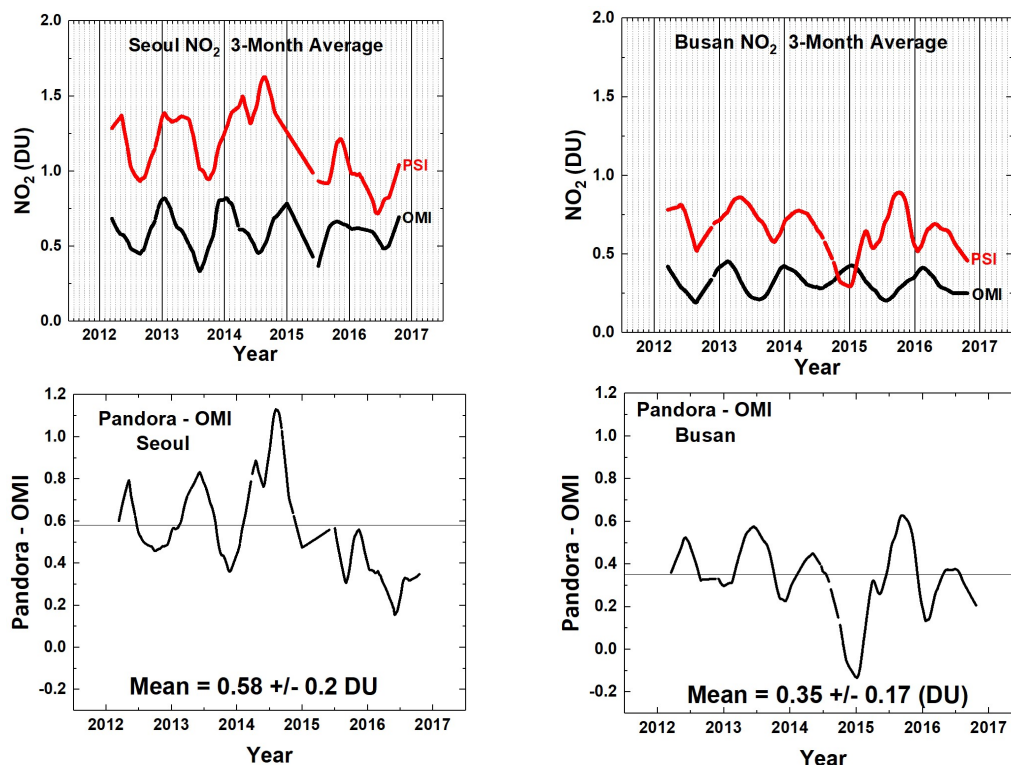


Fig. 9b Comparisons between the seasonal averages for  $C(\text{NO}_2)$  from OMI (black) and PSI (red) at Seoul and Busan for a 5-year period. The lower panels show the seasonal difference between the PSI and OMI.

314



315 Figure 9b shows that the PSI has a mean difference compared to OMI in Busan of 0.35 DU and  
316 peak values (up to 2.5 DU at 13:30 and 4 DU in the late afternoon). The differences could be important  
317 when considering pollution effects on human health (Krafta et al., 2005; Latza et al., 2009). Even larger  
318 differences are observed in Seoul, where the mean difference is 0.58 DU between Pandora and OMI at  
319 the satellite overpass time.  
320

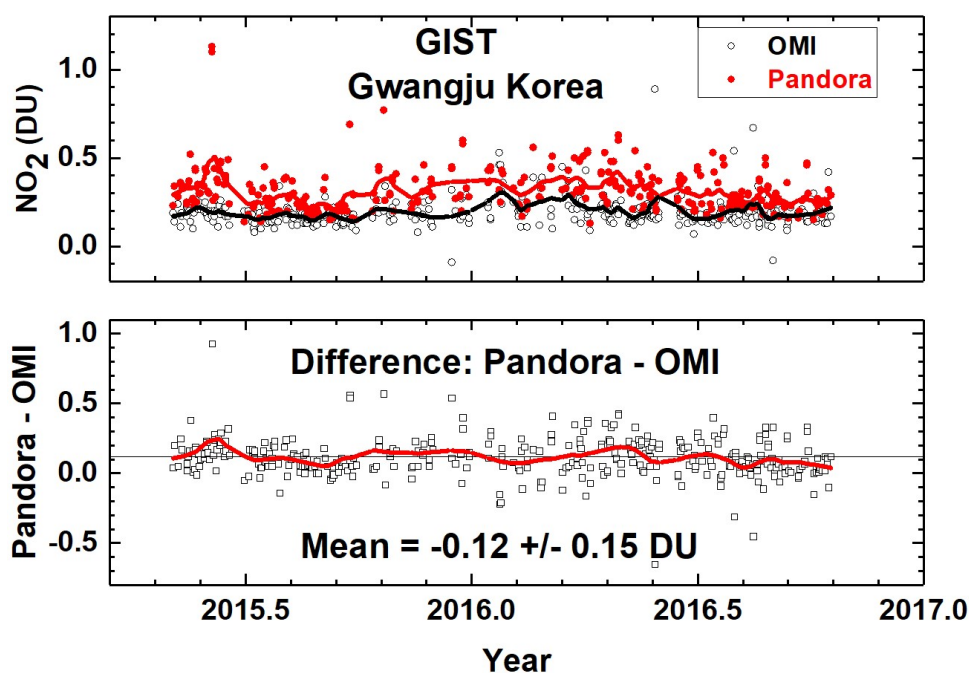


Fig. 10 C(NO<sub>2</sub>) time series from Pandora (red) and OMI (black) for GIST University in Gwangju Korea and their differences. The comparison is formed from time coincidences between Pandora and OMI.

321 A comparison with Lowess(0.1) fits (Locally Weighted least squares fit to 0.1 of the data points,  
322 (Cleveland, 1981)) to the matched Pandora vs OMI overpass data (about 3-month averages) shows that  
323 PSI C(NO<sub>2</sub>) is larger than OMI measured C(NO<sub>2</sub>) mostly because of its much smaller 2<sup>o</sup> field of view (a  
324 circle of 35 meters diameter at 1 km altitude) compared to OMI's FOV of 13 x 24 km<sup>2</sup> at nadir, which  
325 may encompass areas outside of the city or the adjacent ocean areas. For example, the center of Seoul  
326 is about 48 km from the Yellow Sea, while the OMI overpass file lists FOV center distances of over 60 km  
327 from Seoul. Another possible reason for the differences is that OMI C(NO<sub>2</sub>) retrievals use NO<sub>2</sub> vertical  
328 profile shape factors from the low resolution (~110 x 110 km) Global Model Initiative (GMI) model  
329 simulation to calculate air mass factors that are used to determine observed tropospheric NO<sub>2</sub> vertical  
330 columns, while much finer resolution profiles are needed to more accurately represent highly polluted  
331 urban areas such as Seoul. Increases in OMI retrieved tropospheric column NO<sub>2</sub> up to 160 % are found  
332 when using model derived 1.33 x 1.33 km<sup>2</sup> profile shape factors (Goldberg et al., 2017). The effect of  
333 moderate amounts of cloud or aerosol have little effect on the PSI direct -sun spectral fitting retrieval of



334 C(NO<sub>2</sub>) as shown in Fig. 2. OMI and MAXDOAS retrievals are sensitive to the presence of aerosols and  
335 clouds (Kanaya et al., 2014), which may contribute to the underestimate of C(NO<sub>2</sub>) by OMI even after  
336 corrections are made for retrieved aerosol and cloud amounts (Chimot, et al. 2016).

337

338 The implications for assessing clean air indices suggest that OMI underestimates the human  
339 health effect from trace gases such as NO<sub>2</sub>, especially in highly populated urban areas. Figure 5 gives a  
340 much clearer picture of the degree of pollution than is possible with just the 13:30 OMI comparison  
341 measurements, since the late afternoon is the time of maximum pollution.

342

343 The city of Gwangju is much smaller than Busan, with less industrial activity, especially  
344 automobiles. PSI observations at GIST show much closer agreement with OMI (Fig. 10), especially since  
345 GIST is located within the city boundaries, but in an area with much less concentrated industrial activity  
346 compared to the center of Gwangju. The large OMI FOV over a relatively clean area reduce the OMI  
347 difference in measured NO<sub>2</sub> amount compared to the PSI C(NO<sub>2</sub>) amounts. OMI still measures less than  
348 the PSI (0.12 ± 0.15 DU), but the mean difference is not statistically significant. However, OMI clearly  
349 misses the high values of C(NO<sub>2</sub>) that are present in the PSI observations.

350

351

### 352 **5.1 Comparison with 4STAR DC-8 Overpass Data**

353

354 C(NO<sub>2</sub>) results were obtained by the Spectrometer for Sun-tracking Sky-Scanning Atmospheric  
355 Research (4STAR) flown on-board the DC-8 during KORUS-AQ and compared with the PSI (Fig. 11). The  
356 4STAR is an airborne sunphotometer, capable of measuring total C(NO<sub>2</sub>), C(O<sub>3</sub>), water vapor and AOD  
357 columns in its direct-sun mode (Segal-Rozenhaimer et al., 2014; Shinozuka et al., 2013), which is similar  
358 to the mode used by the PSI network.

359

360 A detailed description of 4STAR is given in Dunagan et al., (2013). In brief, the instrument has  
361 two structurally rigid grating array spectrometers that are combined to yield continuous spectra  
362 between 300-1700 nm. The instrument sampling rate is 1 Hz, and the nominal integration time used for  
363 C(NO<sub>2</sub>) retrievals is 50 ms (with six spectra averaged per one sampling period). Dark counts are  
364 measured every 20 min using a shutter mechanism. The 4STAR light collection system has fiber optic  
365 bundle foreoptics that is connected to the spectrometers. A two-axis motion control system with analog  
366 feedback provides active tracking of the solar disk. The instrument full field of view (FOV) is ~1.25°.   
367 C(NO<sub>2</sub>) is retrieved following a method described in Segal-Rozenhaimer et al. (2014), but using the 460-  
368 490 nm spectral range. A series of 4STAR columnar NO<sub>2</sub> values above aircraft (for legs below 300 m)  
369 taken from DC8 “missed approach” maneuvers overflying Olympic Park PSI station, within a radius of 5  
370 km, are shown in Fig. 11. There is a relatively good correlation (R<sup>2</sup>=0.7), with a slight positive bias of  
371 4STAR compared with the PSI values. This might result from higher noise effects (i.e. small amount of  
372 spectra averages) for 4STAR during the fast change of altitude when the aircraft performs its “missed  
373 approach” overpasses over the PSI stations. Relaxing the altitude constraint to include legs below 500 m  
374 showed good agreement with the PSI station at Taewha Mountain, but with an overall lower correlation  
375 coefficient (R<sup>2</sup>=0.54), which is expected due to averaging of larger vertical range. As with PSI, 4STAR



376 shows better agreement with OMI C(NO<sub>2</sub>) for low values of C(NO<sub>2</sub>), but considerable differences over  
377 polluted areas (Segal-Rozenhaimer et al., *in prep.*), when 4STAR C(NO<sub>2</sub>) values are averaged within each  
378 of the OMI pixels corresponding to the flight path for each of the days.  
379

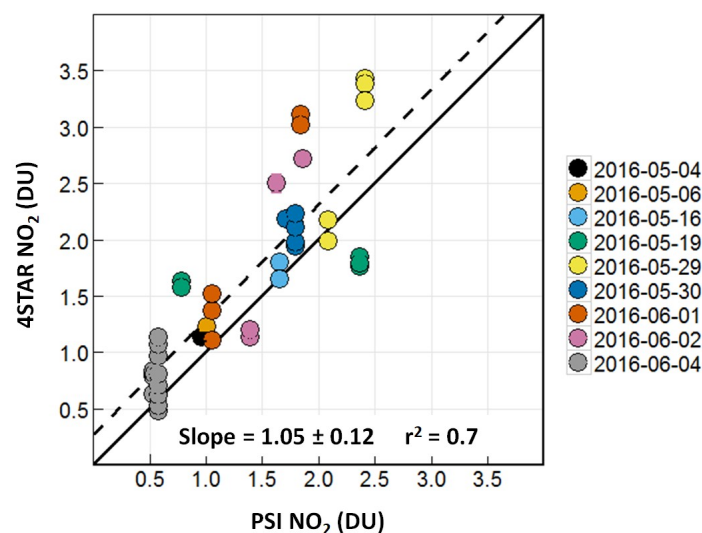


Fig. 11 A correlation plot of C(NO<sub>2</sub>) from 4STAR onboard the DC-8 compared to the C(NO<sub>2</sub>) amount measured by the PSI at Olympic Park on nine different days. The solid black line is the 1:1 line drawn for reference. The dashed line represents the data linear fit, with a slope of 1.05, and a correlation coefficient  $r^2 = 0.7$ , as shown on the plot.

380

381

## 382 6 Formaldehyde from Five Korus-AQ Sites

383

384 PSI makes two sets of direct-sun measurements every 80 seconds. One set is for measurements  
385 in the visible range (380 – 525 nm used for NO<sub>2</sub>) and the other is for the UV range (290 – 380 nm with a  
386 filter, U340, which blocks visible light). Formaldehyde is derived from the same set of spectral  
387 measurements used for ozone (i.e., with a U340 blocking filter), but using the spectral range 332 - 359  
388 nm. Sources of error in the C(HCHO) retrieval arise from the selection of the fitting window and the  
389 amount of C(HCHO) remaining in the reference spectrum after application of the modified Langley  
390 estimation (MLE) method of calibration (Herman et al., 2009, Spinei et al., 2018). The MLE extrapolation  
391 to zero C(HCHO) could have an offset error of 0.1 to 0.2 DU. Selecting different fitting windows can also  
392 cause the C(HCHO) retrievals to differ. For example, a wider alternate fitting window, 324 -360 nm,  
393 retrieves HCHO values that are about 8 % higher because of different amounts of interference from  
394 overlapping absorption by O<sub>3</sub>, NO<sub>2</sub>, and BrO at the spectral resolution of 0.5 to 0.6 nm currently in use.  
395 Absolute offset errors do not affect the retrieval precision (relative column amounts), which is  
396 approximately 0.1 DU.

397



398 The Olympic Park area has much more vegetation than central Seoul for the production of  
399 isoprene (<http://www.olympicpark.co.kr>), which is a significant source of the chemicals needed for  
400 formaldehyde production in the atmosphere (Luecken et al., 2012). Observations from PSI show that  
401 C(HCHO) starts out every day at low levels 0.6 DU at about 08:00 and increases to over 2 DU until 18:00  
402 (Figs 12 and 13). Most HCHO arises from photochemical production, while a significant fraction is  
403 chemically derived from automotive emissions in densely populated urban areas (Friedfeld et al., 2002;  
404 Garcia et al., 2006; Lei et al., 2009; Liteplo et al., 2010). Regardless of the precursor source, HCHO forms  
405 in the atmosphere primarily by photochemistry, which causes HCHO to usually be a minimum early in  
406 the day, increase into the afternoon, and decline towards evening. The PSI C(HCHO) observations (Figs.  
407 12 and 13) support this pattern of daily variation.  
408

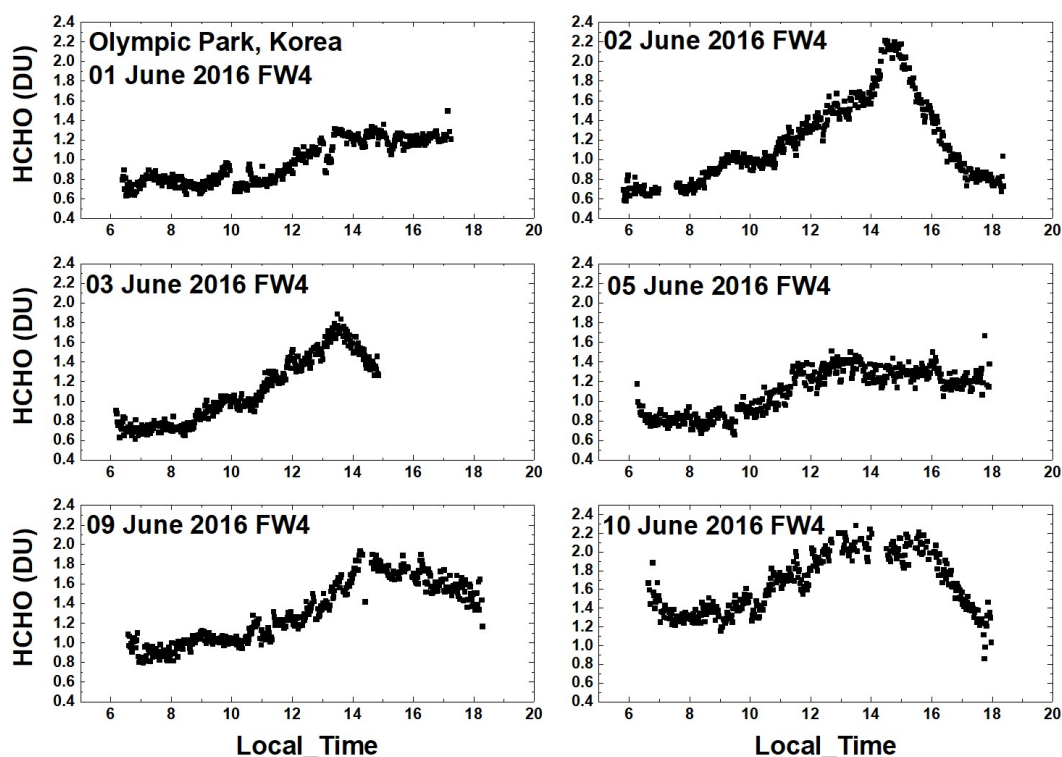


Fig. 12 C(HCHO) from PSI at Olympic Park for 6 days in June 2016. C(HCHO) on 2 June 2016 has a peak value of 2.3 DU at 14:30 hours.

409  
410 A summary of the daily time dependence of C(HCHO) at Olympic Park during the entire  
411 KORUS-AQ campaign is shown in Fig. 13. As in Fig. 12, minimum values are observed in the  
412 morning (06:00 – 08:00) before the chemical and direct sources of HCHO are significant. There  
413 is strong buildup during the day that reached a maximum between 15:00 to 16:00, and then  
414 diminished towards sunset. As with NO<sub>2</sub>, the daily pattern of late afternoon peaking of HCHO



415 amounts presents a problem for polar orbiting satellite observations (e.g., OMI observations at  
 416 13:30) assessing air quality.  
 417  
 418  
 419

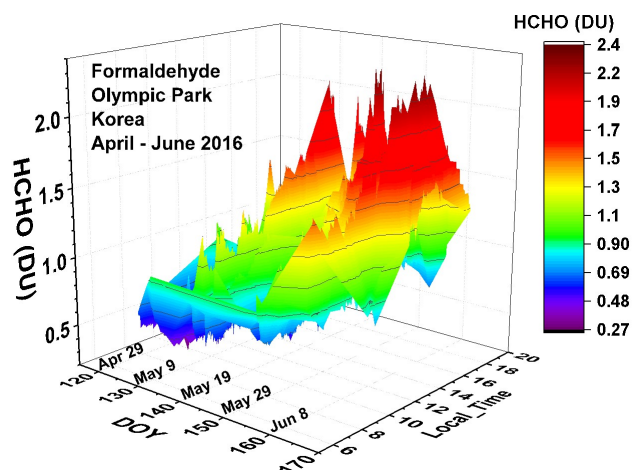


Fig. 13 Pandora measured formaldehyde amounts vs day of the year and local time for 29 April 2016 to 11 June 2016 in Olympic Park.

420

421 Figure 14 shows two altitude profiles acquired by the Compact Atmospheric Multispecies  
 422 Spectrometer (CAMS) (Richter et al., 2015) onboard the DC-8 aircraft as it spiraled over the  
 423 Olympic Park area on 4 May 2016 in the morning and at midday.

424

425 The morning integrated amount on 4 May was  $1.02 \times 10^{16}$  molecules  $\text{cm}^{-2}$  (0.38 DU) and the  
 426 afternoon amount was  $6.95 \times 10^{15}$  molecules  $\text{cm}^{-2}$  (0.26 DU), both substantially less than the PSI  
 427 measured values of 0.48 DU and 0.42 DU, respectively. There were no surface measurements of HCHO  
 428 mixing ratio on 4 May at Olympic Park. On 2 June at 11:40 there was a surface measurement 3.94 ppb.  
 429 Including the surface measurement in the profile integral yields  $\text{Integ}(0.026, 7.2) = 0.55$  DU, while PSI  
 430 measured 1.2 DU, which is consistent with the differences shown in Fig. 14. The notation in Fig 14 is

431 
$$\text{Integ}(z_1, z_2) = \int_{z_1}^{z_2} \text{HCHO}(z) dz$$
 for the altitudes  $z_1$  to  $z_2$ .

432

433

434

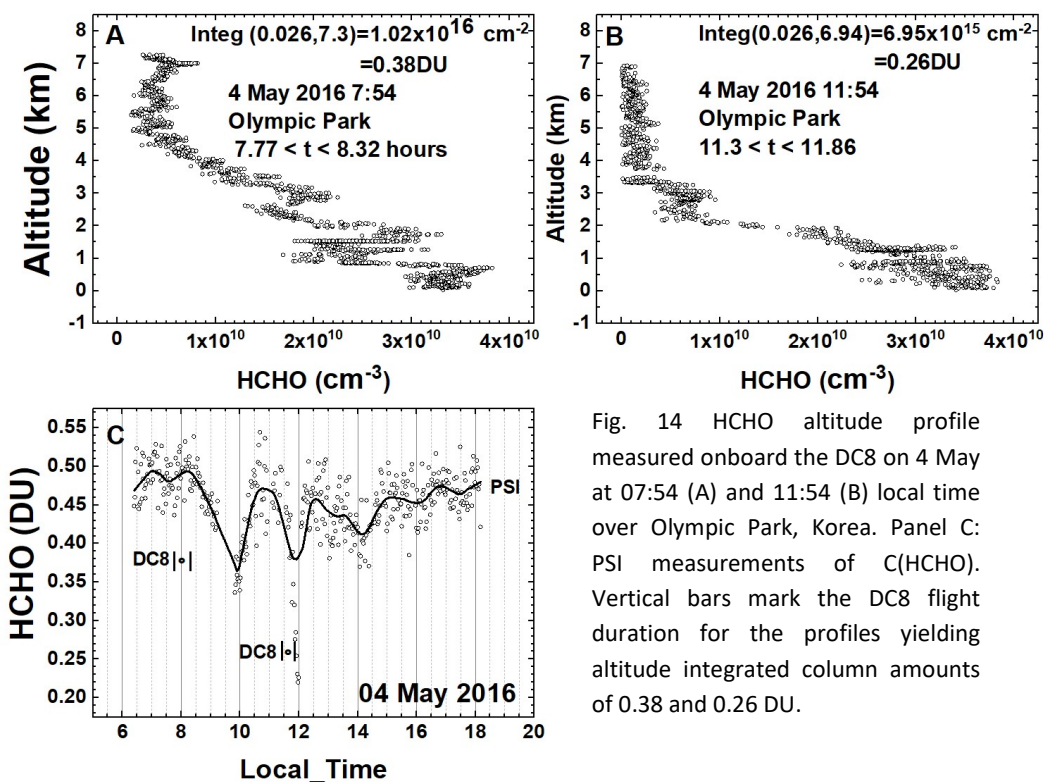


Fig. 14 HCHO altitude profile measured onboard the DC8 on 4 May at 07:54 (A) and 11:54 (B) local time over Olympic Park, Korea. Panel C: PSI measurements of C(HCHO). Vertical bars mark the DC8 flight duration for the profiles yielding altitude integrated column amounts of 0.38 and 0.26 DU.

435 The profiles used data for lower altitudes obtained from aircraft “missed approach”  
 436 maneuvers at a nearby Seoul Airbase, 8.5 km from Olympic Park, (Fig. 15). When available, a  
 437 single surface altitude point was added using ground-based volume mixing ratio measurements  
 438 obtained from US Environmental Protection Agency measurements using quantum cascade  
 439 laser instruments (Hottle et al., 2009, Spinei et al., 2018 and references therein). The DC-8 minimum  
 440 altitude exactly over Olympic Park was typically around 0.4 km above the surface (black circles  
 441 Fig. 15). Large vertical DC-8 HCHO gradients were observed as the DC8 descended to lower  
 442 altitudes over Seoul Airbase. A comparison of 10-second DC-8 HCHO averages at the points of  
 443 closest spatial approach to the Olympic Park (black circles) site on June 4, for example, to peak  
 444 HCHO measurements during missed approaches at the nearby Seoul Airbase (20 – 40 meters  
 445 above the ground) revealed ratios in the observed HCHO (black circles) ranging between 75 % to  
 446 83 % of the maximum values near the surface. Since Olympic Park DC-8 overpasses miss  
 447 significant near surface HCHO amounts, the profiles shown in Figs. 14 and 16 incorporate the  
 448 HCHO amounts down to the surface at an altitude of 0.026 km asl derived from the “missed  
 449 approach” at Seoul airbase. HCHO measurements above the maximum altitude over Olympic  
 450 Park (see Fig. 14 and 16) were taken from the closest time over the Taewha Mtn. site, 28 km



451 from Olympic Park. The assumption is that the horizontal gradients above 2.2 km (Fig. 15) can  
452 be neglected,  
453

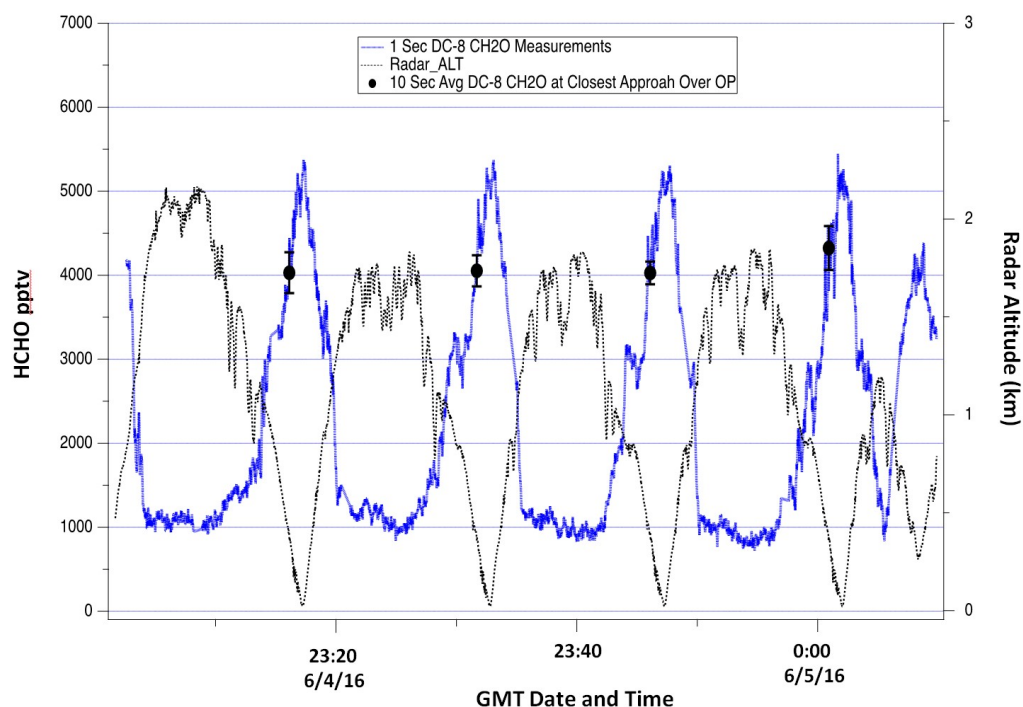


Fig. 15 DC-8 HCHO measurements over Olympic Park on June 4. The continuous blue profiles show the 1-second HCHO data while the black points with error bars show the 10-second average and standard deviation of this data at points of closest approach above the Olympic Park site.

454

455 After conversion from mixing ratio to molecules/cm<sup>3</sup> using the measured atmospheric  
456 density, the resulting profile data were integrated from the minimum (0.026 km asl, Table 1) to  
457 the maximum heights indicated in Fig. 14. The result is 0.38 DU at 07:54 and 0.26 DU at 11:54  
458 compared to the measurements from the Pandora instrument 0.48 and 0.38 DU. The derived  
459 vertical HCHO columns from the DC8 data in Fig. 14 A and B are 79 % of PSI measured C(HCHO) in the  
460 morning and 68 % of PCI C(HCHO) at midday (Fig 14 C).

461

462 A similar comparison is shown in Fig. 16 for 5 June 2016 where the amount of C(HCHO)  
463 is much larger than on 4 May. Integration of the measured profiles yields column densities of  
464 0.60 and 0.82 DU at 08:30 and 15:21 hours. For this case, at both times the DC8 values are  
465 about 77 % and 63 % of the PSI measured column amounts, 0.78 and 1.3 DU. For both cases in



466 Figs. 14 and 15 the 23 % to 37 % differences are outside of the expected error from PSI fitting  
467 window selection and from residual HCHO included in the MLE calibration method.  
468

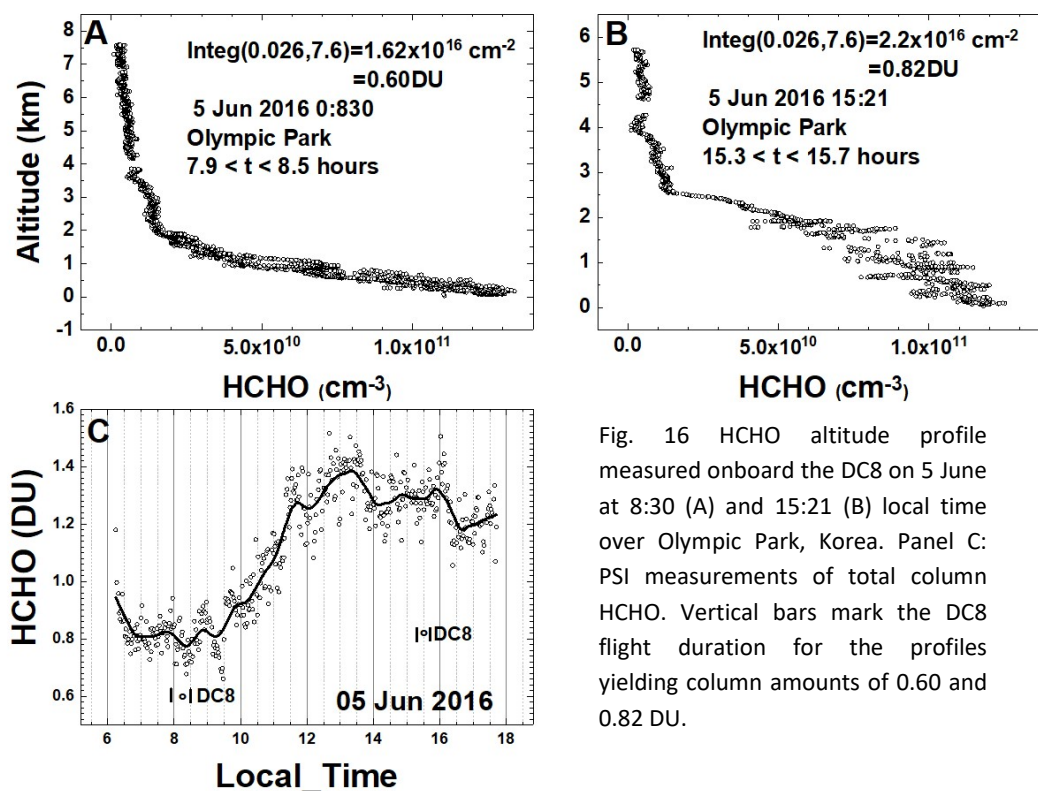


Fig. 16 HCHO altitude profile measured onboard the DC8 on 5 June at 8:30 (A) and 15:21 (B) local time over Olympic Park, Korea. Panel C: PSI measurements of total column HCHO. Vertical bars mark the DC8 flight duration for the profiles yielding column amounts of 0.60 and 0.82 DU.

469  
470 Another Olympic Park case on 9 June 2016 shows DC8=0.79 vs PSI=1 DU at 08:06,  
471 DC8=0.74 vs PSI=1.3 DU at 12:12, and DC8=1.13 vs PSI=1.9DU, or the DC8 measurements are 79  
472 % and 57 % less than the PSI total column HCHO. All of the remaining comparisons of DC8  
473 profile results with PSI C(HCHO) show similar results. The reasons for the disagreement between  
474 C(HCHO) measured by direct sun observations (PSI) and the integrated column density from aircraft  
475 measurements of HCHO VMR are not known. Contributions to the differences include the selection of  
476 the PSI wavelength window (332 - 359 nm) and possible interference from overlapping NO<sub>2</sub> and O<sub>3</sub>  
477 absorption that are not properly included, and, more likely, the use of CAMS measured volume mixing  
478 ratios at the lowest altitudes from the nearby Seoul airbase, 8.5 km from Olympic Park, where spatial  
479 variation may affect the calculation of C(HCHO). The use of Taehwa Mtn. data for higher altitudes over  
480 Olympic Park contributes 25 % for 3 of the above cases and 50 % for 4 May 2016 at 07:54 (Fig.  
481 14A). This is probably not the reason for the disagreement between CAMS and PSI, since the percent  
482 underestimate for CAMS over Taehwa is about the same magnitude (Table 2) as over Olympic Park.  
483



484 PSI measurements show that Olympic Park produces more HCHO almost every day than  
 485 observed at the Yonsei University in Seoul and Taehwa Mountain sites (Figs. 12, 17, 18). The  
 486 hourly variations observed during the KORUS-AQ campaign at the Yonsei University in Seoul  
 487 and at Taehwa Mountain sites are similar to Olympic Park even though most of the HCHO is  
 488 locally produced by photochemistry, but has a relatively short lifetime of a few hours in  
 489 polluted air where there is significant ozone and OH. However, at typical wind speeds of 10 -20  
 490 km/hour and a chemical lifetime of 2.5 hours (Dufour et al., 2009), HCHO can be transported  
 491 about 25 – 50 km, which is far enough for some transport of HCHO between the PSI sites at  
 492 Yonsei, Olympic Park, and Taehwa Mtn. DC8 CAMS results over the Taehwa Mtn. site compared  
 493 to PSI are given in Table 2 with differences similar to Olympic Park.  
 494

Table 2 Taehwa Mtn DC8 compared to PSI measurements in Fig. 18

| Date   | LT       | DC8 HCHO DU | PSI HCHO | Percent |
|--------|----------|-------------|----------|---------|
| 11 May | 08:25:19 | 0.4         | 0.6      | 67      |
| 18 May | 08:34:26 | 0.4         | 0.5      | 80      |
| 30 May | 12:05:00 | 0.5         | 0.9      | 56      |
| 10 Jun | 08:22:45 | 1           | 1.16     | 86      |
| 10 Jun | 12:22:53 | 1           | 1.5      | 67      |
| 10 Jun | 15:46:03 | 1           | 1.3      | 77      |

495

496

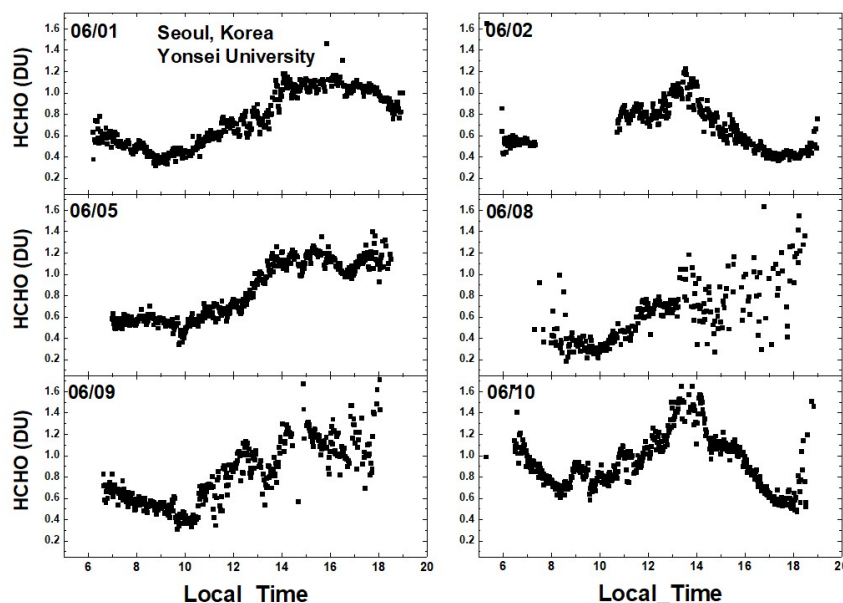


Fig. 17 Total column HCHO from Pandora Yonsei University, Seoul for 6 days in June 2016. C(HCHO) on 2 June 2016 has a peak value of 1.2 DU at 13:30 hours.

497



498  
499

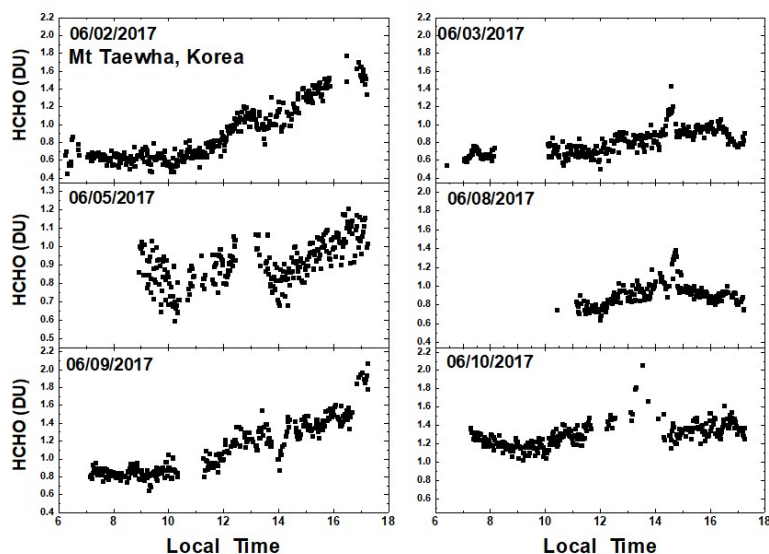


Fig. 18 Total column HCHO from Pandora Taehwa Mountain for 6 days in June 2016. C(HCHO) on 2 June 2016 has a peak value of 1.7 DU at 16:20.

500

501

502

Figure 19a and 19b summarizes all of the C(HCHO) data obtained during KORUS-AQ at the five sites. The graphs on the left show all of the data points (light gray circles) as a function of the local time and a Lowess(0.1) fit to the data showing the average hourly behavior. The spread of the data about the Lowess(0.1) fit represents the day-to-day variation at a given local time. On average, Mt. Taehwa tends to increase throughout each day, while Yonsei and Olympic Park show maxima at 14:00 and 15:30, respectively. Similarly, in Fig. 18b Yeogju increases during the day having a maximum at 17:42 while Anmyeondo has a broad peak with maxima at 12:00 and 13:42.

506

507

508

509

510

511

The histograms on the right side of Fig. 19 represent the percent frequency of occurrence of C(HCHO) in 0.1 DU bins. C(HCHO) at Mt. Taehwa and Seoul rarely exceeds 1.5 DU compared to Olympic Park where C(HCHO) > 2 DU for a significant fraction of time. The most frequent values are 0.6 DU for Seoul, 0.9 DU for Mt Taehwa, and over 1 DU for Olympic Park. Olympic Park also has a broader distribution towards higher values of C(HCHO) than other sites.

512

513

514

515

516

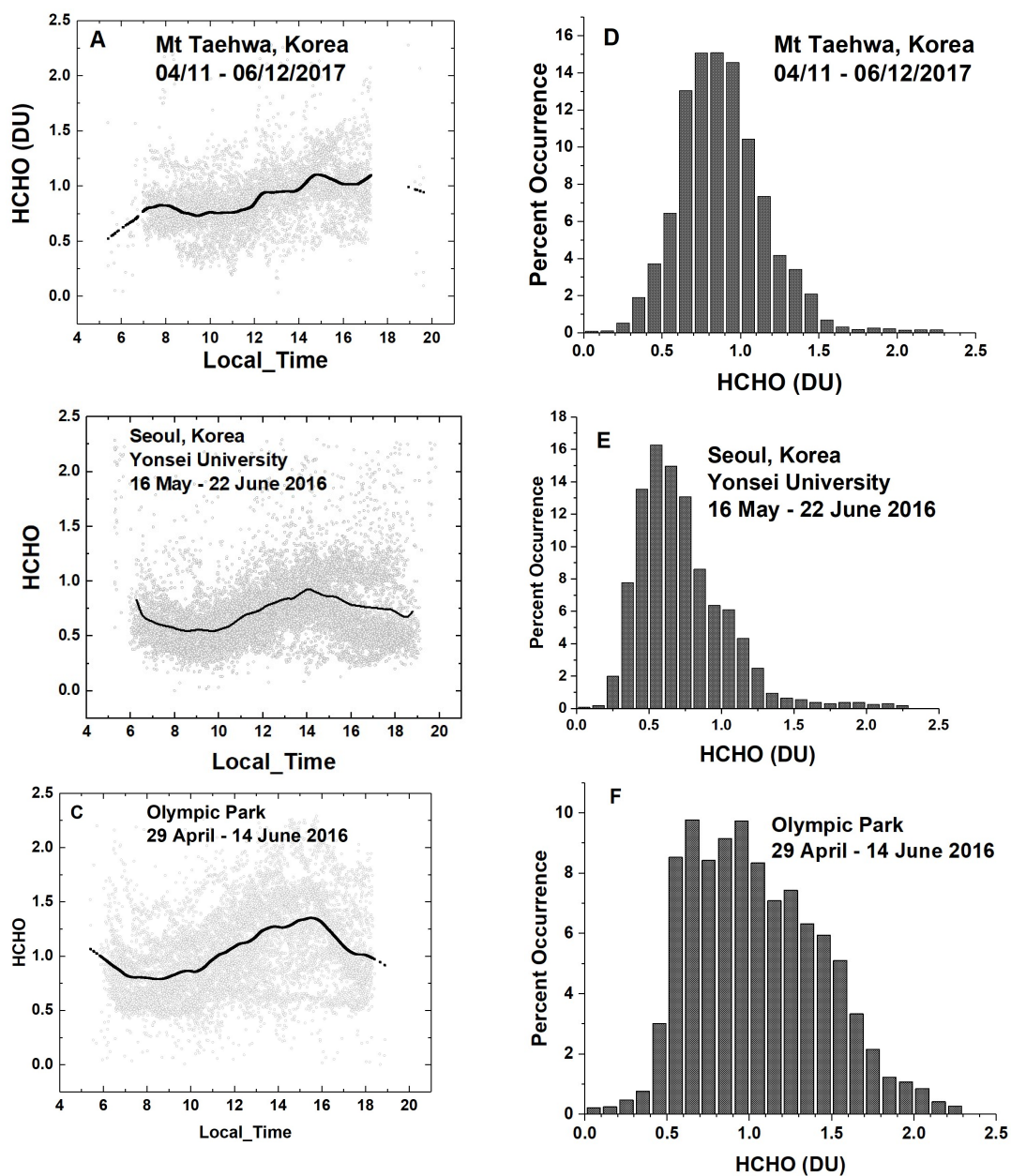


Fig. 19a Summary of total column HCHO for the stated dates during the KORUS-AQ campaign. The solid line is a Lowess(0.1) fit to the data. The sharp cutoffs in panel A, B, and C were caused by obstructions of the direct sun from the PSI FOV in the afternoon.



518

519

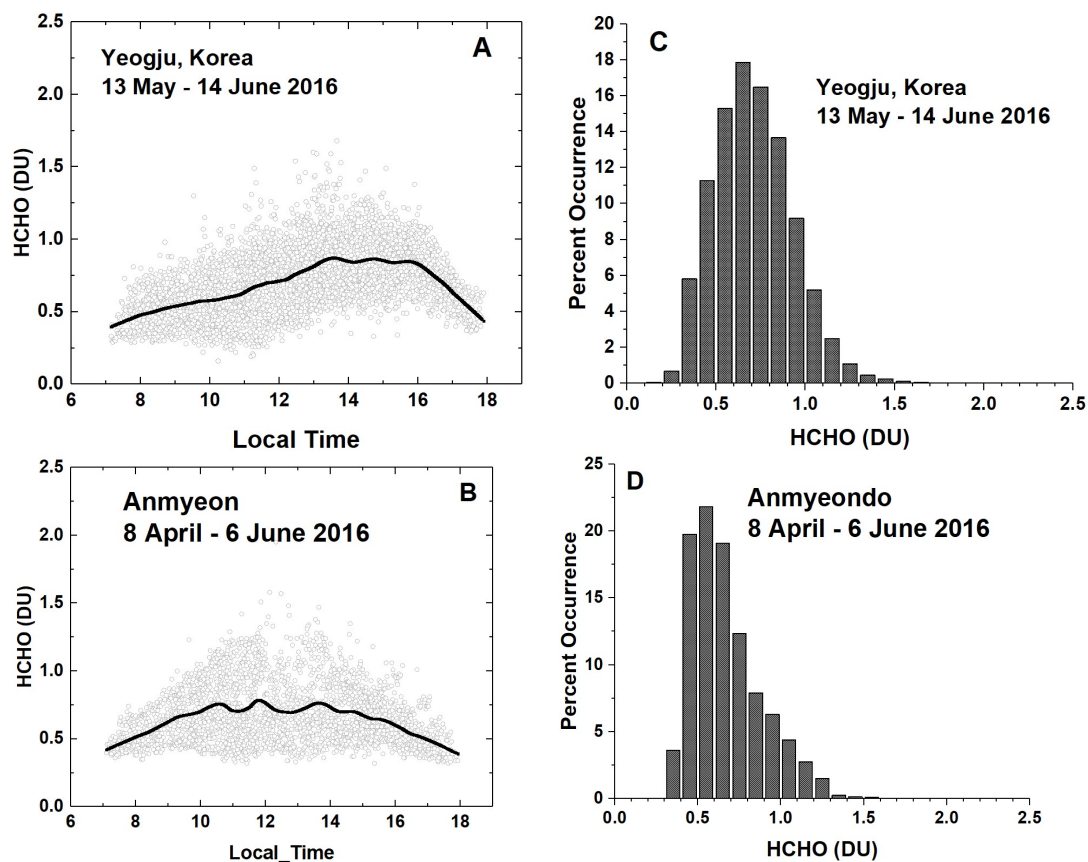


Fig. 19b Summary of total column HCHO for the stated dates during the KORUS-AQ campaign. Panels A and B represent the daily variation at a given local time. The solid line is a Lowess(0.1) fit to the data. Panels C and D show the frequency of occurrence (%) for different amounts of HCHO.

520

521 The general intra-day C(HCHO) time dependence and C(HCHO) percent occurrence are  
522 shown for two additional sites (Fig. 19b), Yeogju and Anmyeondo. Yeogju shows an increase in  
523 C(HCHO) from morning to a peak value of 0.85 DU at 14:42, which then declines after 16:00. In  
524 contrast, Anmyeondo is almost symmetric with the sun position, having a maximum of about  
525 0.77 DU near 12:00 and 13:42 hours.

526



527 The average change in C(HCHO) during the spring campaign at the five sites is  
528 summarized in Fig. 20. Of the sites, Olympic Park showed the largest change rate, 58 %/Month  
529 followed by Amnyeondo at 50 %/Month, then Taehwa (33 %/Month), Yonsei Seoul (25  
530 %/Month), and Yeogju (-13 %/Month). Amnyeondo tends to have lower C(HCHO) amounts  
531 because of its relatively isolated coastal location. These 2-month trends include seasonal  
532 increases during the campaign months May and June, 2016.

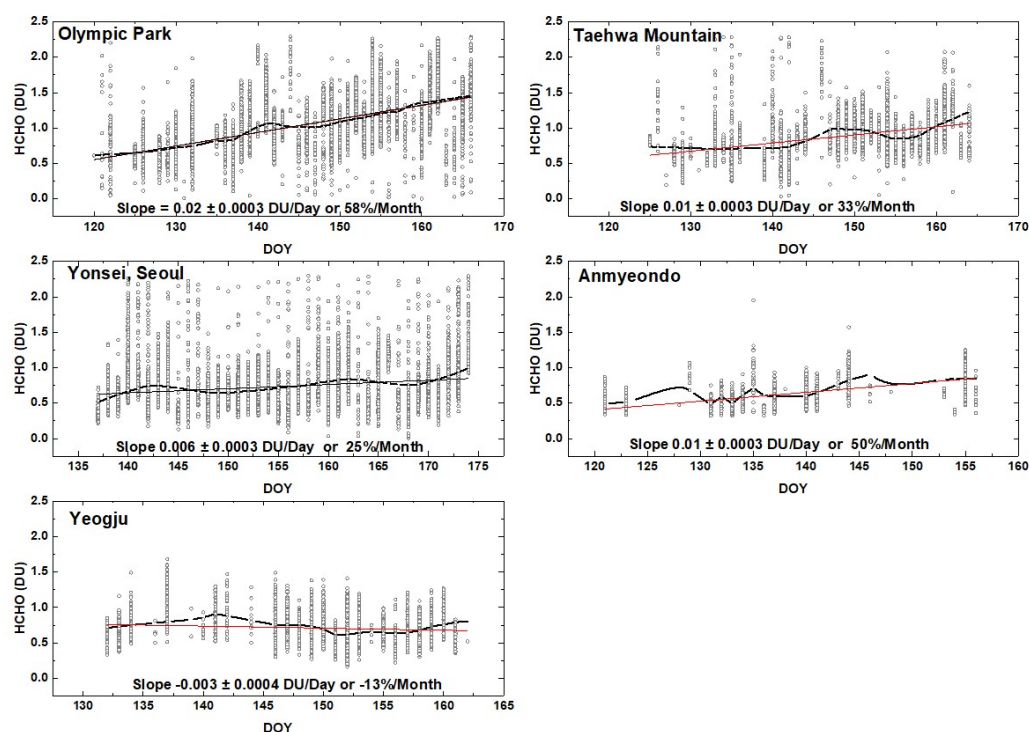


Fig. 20 The springtime change in C(HCHO) over about a 40 day period depending on the site. The “vertical bars” are the diurnal variation within each day of data. The thicker red curve is a Lowess(0.3) fit to the data, while the thin red line is a linear least squares fit. The Lowess(0.3) fit is approximately a 10-day local least-squares average.



533 It is difficult to compare PSI C(HCHO) with OMI for the KORUS-AQ period, since OMI  
 534 overpass C(HCHO) data for 2016 have some missing days (Fig. 21). For days with matching  
 535 data points over Seoul, PSI C(HCHO) (approximately 0.8 DU) is almost always larger than the  
 536 OMI values (0.2 DU) plus a few very high PSI values and two high OMI values. The general  
 537 day-to-day variations are similar.  
 538

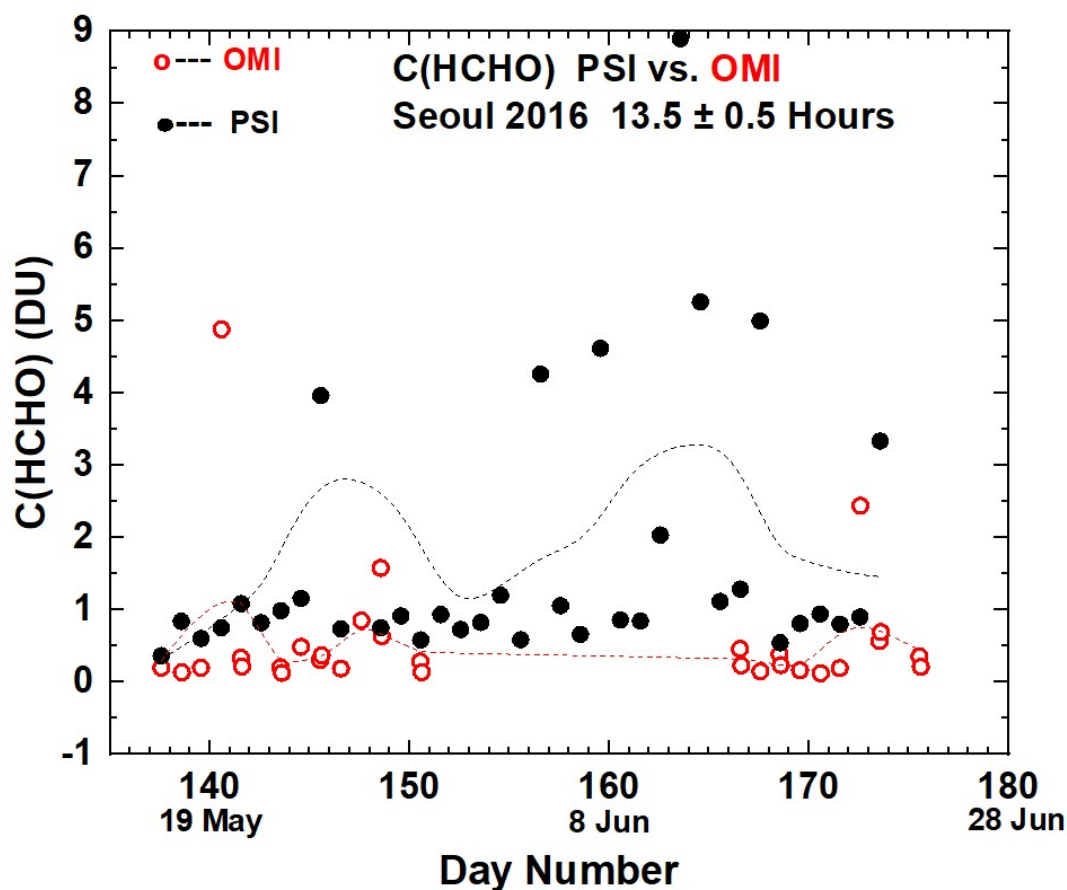


Fig. 21 Compare PSI • and OMI ◦ retrievals of C(HCHO) at  $13.5 \pm 0.5$  hours. OMI overpass data, V03, are from <https://avdc.gsfc.nasa.gov/index.php?site=1113974256&id=81>

539

540 **7 Summary**

541

542 Nine Pandora Spectrometer Instruments, PSI, were installed at 8 sites in South Korea as part of  
 543 the KORUS-AQ ground, aircraft, and satellite measurements for air-quality studies. The measurements



544 made during the months of April to June by PSI showed that are very high amounts of urban pollution  
545 from NO<sub>2</sub> and HCHO, and more moderate, but still high values, away from the urban centers. An  
546 exception was Amnyeondo, which is located on a west-coastal island adjacent to the Yellow Sea about  
547 100 km south of Seoul. The urban areas show minimum values in the morning that rise rapidly  
548 throughout the day, peaking in the late afternoon for both C(NO<sub>2</sub>) and C(HCHO).

549

550 PSI direct-sun retrieved values of C(NO<sub>2</sub>) and C(HCHO) are always larger than OMI retrieved  
551 C(NO<sub>2</sub>) and C(HCHO) for the OMI overpass times ( $13.5 \pm 0.5$  hours). In urban areas, PSI C(NO<sub>2</sub>) averages  
552 are at least a factor of two larger than OMI averages. Similar differences are seen for C(HCHO) in Seoul.  
553 However, late afternoon values measured by PSI are even larger, implying that OMI measurements  
554 underestimate the effect of poor air quality on human health. The primary cause of the OMI  
555 underestimate is the large OMI FOV that includes regions containing low values of pollutants. In  
556 relatively clean areas, PSI and OMI are more closely in agreement.

557

558 PSI retrieved C(NO<sub>2</sub>) amounts for Seoul frequently exceed 2 DU and occasionally reach 6 DU.  
559 Other urban centers in the south, Busan and Gwangju, have smaller C(NO<sub>2</sub>) amounts, but exhibit a  
560 similar strong diurnal pattern, namely low values in the morning and high values later during midday.  
561 This behavior is expected because of the large number of urban automobiles and concentrated industry.  
562 Urban areas downwind from Seoul show high C(NO<sub>2</sub>) amounts, but also show daily minimum amounts in  
563 the morning that increase later in the day. Two of the sites, Seoul and Busan, have long-term C(NO<sub>2</sub>)  
564 data records, 2012 – 2016, that suggest a gradual decrease in C(NO<sub>2</sub>) amounts in Korea. When  
565 compared with OMI, both ground-based PSI's and the 4STAR aircraft instrument onboard the DC8 show  
566 that the correlation is best for small values of C(NO<sub>2</sub>), most often seen in the troposphere and  
567 stratosphere and worst for high values that are usually in the boundary layer near their local sources. In  
568 Olympic Park, the measurements of significant values of C(HCHO) and high values of C(NO<sub>2</sub>) in the  
569 afternoon suggest that there are increased boundary layer amounts of ozone.

570

571 C(HCHO) amounts were obtained for five sites, Yonsei University in Seoul, Olympic Park, Taehwa  
572 Mtn., Amnyeondo, and Yeosu. Of these the largest amounts of C(HCHO) were observed at Olympic Park,  
573 and Taehwa Mountain, both surrounded by significant amounts of vegetation. Comparisons of PSI  
574 results were made with overflights on the DC8 aircraft for Taehwa Mtn and Olympic Park showing a  
575 significant difference in total column HCHO. In all cases, PSI measured substantially more C(HCHO) than  
576 obtained from integrating the altitude profiles measured from the DC8 overflights.

577



578 **Data Sources**

579 **OMI Formaldehyde HCHO Version 03:** <https://avdc.gsfc.nasa.gov/index.php?site=1113974256&id=81>

580 **OMI Nitrogen Dioxide NO<sub>2</sub> Version 03** <https://avdc.gsfc.nasa.gov/index.php?site=666843934&id=13>

581 **Pandora KORUS-AQ** <https://avdc.gsfc.nasa.gov/pub/DSCOVER/Pandora/DATA/KORUS-AQ/>

582



583 **Author Contributions**

584

585 Jay Herman: Wrote most of the paper and performed the analysis and comparisons with the DC-8  
586 aircraft measurements

587 Elena Spinei: Derived the formaldehyde altitude profiles suitable for comparison with Pandora data

588 Alan Fried: Obtained the HCHO profile data from the DC-8 CAMS instrument

589 Jhoon Kim: Provided support for the installation of Pandora instruments in Korea.

590 Jae Kim: Provided support for the Pandora located in Busan .

591 Woogyung Kim: Provided support in installing the Pandoras and analyzing the raw data

592 Alexander Cede: Provided calibration and data analysis support

593 Nader Abuhassan: Provided Pandora setup in Korea and provided the maintenance of calibration

594 Michal Segal-Rozenhaimer: Provided the 4STAR NO<sub>2</sub> data from the DC-8 flights and the comparison with  
595 Pandora

596

597 The authors declare that they have no conflict of interest.

598 **8 References**

- 599 Boersma, K. F., D. J. Jacob, M. Trainic, Y. Rudich, I. DeSmedt, R. Dirksen, and H. J. Eskes, Validation of  
600 urban NO<sub>2</sub> concentrations and their diurnal and seasonal variations observed from the SCIAMACHY and  
601 OMI sensors using in situ surface measurements in Israeli cities, *Atmos. Chem. Phys.*, 9, 3867–3879,  
602 2009.
- 603 Chimot, J., Vlemmix, T., Veeffkind, J. P., de Haan, J. F., and Levelt, P. F.: Impact of aerosols on the OMI  
604 tropospheric NO<sub>2</sub> retrievals over industrialized regions: how accurate is the aerosol correction of cloud-  
605 free scenes via a simple cloud model?, *Atmos. Meas. Tech.*, 9, 359-382, [https://doi.org/10.5194/amt-9-](https://doi.org/10.5194/amt-9-359-2016)  
606 359-2016, 2016.
- 607 Cleveland, William S., LOWESS: A program for smoothing scatterplots by robust locally weighted  
608 regression. *The American Statistician*. **35** (1): 54. [JSTOR 2683591](https://doi.org/10.2307/2683591). [doi:10.2307/2683591](https://doi.org/10.2307/2683591), 1981.  
609
- 610 Dufour, G., F. Wittrock, M. Camredon, M. Beekmann, A. Richter, B. Aumont, and J. P. Burrows,  
611 SCIAMACHY formaldehyde observations: constraint for isoprene emission estimates over Europe?,  
612 *Atmos. Chem. Phys.*, 9, 1647–1664, 2009  
613
- 614 Dunagan, S. E., R. Johnson, J. Zavaleta, P. B. Russell, B. Schmid, C. Flynn, J. Redemann, Y. Shinozuka, J.  
615 Livingston, and M. Segal-Rosenhaimer, 4STAR spectrometer for sky-scanning Sun-tracking atmospheric  
616 research: Instrument technology, *Remote Sens. (Special Issue*  
617 "Optical Remote Sensing of the Atmosphere"), 5, 3872–3895, doi:10.3390/rs5083872, 2013.
- 618 Fried, A., Walega, J. G., Olson, J. R., Crawford, J. H., Chen, G., Weibring, P., ... Millet, D. B. (2008).  
619 Formaldehyde over North America and the North Atlantic during the summer 2004 INTEX campaign:  
620 Methods, observed distributions, and measurement-model comparisons. *Journal of Geophysical*  
621 *Research*, 113(D10). <https://doi.org/10.1029/2007JD009185>, 2008.
- 622 Friedfeld, S., M. Fraser, K. Ensor, S. Tribble, D. Rehle, D. Leleux, F. Tittel Statistical analysis of primary and  
623 secondary atmospheric formaldehyde, *Atmospheric Environment*, 36, 4767-4775, 2002.
- 624 Garcia, A. R., R. Volkamer, L. T. Molina, M. J. Molina, J. Samuelson, J. Mellqvist, B. Galle, S. C. Herndon, C. E.  
625 Kolb, Separation of emitted and photochemical formaldehyde in Mexico City using a statistical analysis  
626 and a new pair of gas-phase tracers *Atmospheric Chemistry Physics*, 6, 4545-4557, 2006.
- 627 Goldberg D. et al., (2017), A High-Resolution And Observationally Constrained Omi NO<sub>2</sub> Satellite  
628 Retrieval, *Atmos. Chem. Phys. Discuss.*, doi:10.5194/acp-2017-219, 2017.
- 629 Herman, Jay, Alexander Cede, Elena Spinei, George Mount, Maria Tzortziou, Nader Abuhassan, NO<sub>2</sub>  
630 Column Amounts from Ground-based Pandora and MFDOAS Spectrometers using the Direct-Sun DOAS  
631 Technique: Intercomparisons and Application to OMI Validation, *J. Geophys. Res.*, 114, D13307,  
632 doi:10.1029/2009JD011848, 2009.
- 633 Kanaya, Y., Irie, H., Takashima, H., Iwabuchi, H., Akimoto, H., Sudo, K., Gu, M., Chong, J., Kim, Y. J., Lee,  
634 H., Li, A., Si, F., Xu, J., Xie, P.-H., Liu, W.-Q., Dzhola, A., Postlyakov, O., Ivanov, V., Grechko, E.,



- 635 Terpuogova, S., and Panchenko, M.: Long-term MAX-DOAS network observations of NO<sub>2</sub> in Russia and  
636 Asia (MADRAS) during the period 2007–2012: instrumentation, elucidation of climatology, and  
637 comparisons with OMI satellite observations and global model simulations, *Atmos. Chem. Phys.*, **14**,  
638 7909-7927, <https://doi.org/10.5194/acp-14-7909-2014>, 2014.
- 639 Kim, Na Kyung, Yong Pyo Kim, Yu Morino, Jun-ichi Kurokawa, Toshimasa Ohara, Verification of NOx  
640 emission inventory over South Korea using sectoral activity data and satellite observation of NO<sub>2</sub> vertical  
641 column densities, *Atmospheric Environment*, **77**, 496-508, 2013.
- 642 Krafta, Martin, Thomas Eikmannb, Andreas Kapposc, Nino Künzlid, Regula Rappe, Klaus Schneiderf,  
643 Heike Seitzb, Jens-Uwe Voss, H.-Erich Wichmannh, he German view: Effects of nitrogen dioxide on  
644 human health – derivation of health-related short-term and long-term values, *International Journal of*  
645 *Hygiene and Environmental Health*, **208**, 305–318, 2005.
- 646 Kramer, L.J., R. J. Leigh, J. J. Remedios, et al., “Comparison of OMI and Ground-Based in situ and  
647 MAXDOAS Measurements of Tropospheric Nitrogen Dioxide in An Urban Area,” *J. Geophys. Res.* **113**,  
648 D16S39, 2008.
- 649 Latza, Ute, , Silke Gerdes, and Xaver Baur, ffects of nitrogen dioxide on human health: Systematic review  
650 of experimental and epidemiological studies conducted between 2002 and 2006, *International Journal*  
651 *of Hygiene and Environmental Health* **212**,Pages 271 - 287, [doi.org/10.1016/j.ijheh.2008.06.003](https://doi.org/10.1016/j.ijheh.2008.06.003), 2009.
- 652 Lei, W., Zavala, M., de Foy, B., Volkamer, R., Molina, M. J., and Molina, L. T.: Impact of primary  
653 formaldehyde on air pollution in the Mexico City Metropolitan Area, *Atmos. Chem. Phys.*, **9**, 2607–2618,  
654 2009.
- 655 Liteplo, R.G., R. Beauchamp, M.E. Meek, and R. Chénier. Formaldehyde. Geneva: International  
656 Programme on Chemical Safety; 2002. [18 May 2010]. (Concise International Chemical Assessment  
657 Document 40) ( <http://www.inchem.org/documents/cicads/cicads/cicad40.htm>).
- 658 Luecken, D.J., W.T. Hutzell, M.L. Strum, G.A. Pouliot, Regional sources of atmospheric formaldehyde and  
659 acetaldehyde, and implications for atmospheric modeling, *Atmospheric Environment* **47**, 477-490,  
660 [doi:10.1016/j.atmosenv.2011.10.005](https://doi.org/10.1016/j.atmosenv.2011.10.005), 2012.
- 661 Meller, Richard, and Geert K Moortgat. Temperature dependence of the absorption cross sections of  
662 formaldehyde between 223 and 323 k in the wavelength range 225-375 nm. *Journal of Geophysical*  
663 *Research: Atmospheres* (19842012), **105**(D6):70897101, 2000.
- 664
- 665 Richter D., P. Weibring, J. G. Walega, A. Fried, S. M. Spuler, M. S. Taubman: Compact highly sensitive  
666 multi-species airborne mid-IR spectrometer, *Appl. Phys. B*, [doi: 10.1007/s00340-015-6038-8](https://doi.org/10.1007/s00340-015-6038-8), 2015.
- 667 Russell, A. R., Perring, A. E., Valin, L. C., Bucsela, E. J., Browne, E. C., Wooldridge, P. J., and Cohen, R. C.: A  
668 high spatial resolution retrieval of NO<sub>2</sub> column densities from OMI: method and evaluation, *Atmos.*  
669 *Chem. Phys.*, **11**, 8543-8554, 2011.



- 670 Segal-Rosenheimer, M., P. B. Russell, B. Schmid, J. Redemann, J. M. Livingston, C. J. Flynn, R. R. Johnson,  
671 S. E. Dunagan, Y. Shinozuka<sup>1</sup>, J. Herman, A. Cede, N. Abuhassan, J. M. Comstock, J. M. Hubbe, A.  
672 Zelenyuk<sup>3</sup>, and J. Wilson, (2014) Tracking elevated pollution layers with a newly developed  
673 hyperspectral Sun/Sky spectrometer(4STAR): Results from the TCAP 2012 and 2013 campaigns, J.  
674 Geophys. Res. Atmos., 119, 2611–2628, doi:10.1002/2013JD020884, 2014.
- 675 Shinozuka, Y., et al. , Hyperspectral aerosol optical depths from TCAP flights, J. Geophys. Res. Atmos.,  
676 118, 12,180–12,194, doi:10.1002/2013JD020596, 2013.
- 677 Spinei, E., N. Abuhassan, A Cede, M. Tiefengraber, M. Mueller, J. Herman, N. Nowak, B. Poche, S. Choi<sup>7</sup>,  
678 A. Whitehill, J. Szykman, V. Lukas, D. Williams, R. Long, Jin Liao, Jason St. Clair, Glenn Wolfe, Thomas  
679 Hanisco, Changmin Cho, Alan Fried, Petter Weibring, Dirk Richter, Robert Swap, James Walega, Pandora  
680 formaldehyde measurements during KORUS-AQ over Olympic Park and Taehwa (South Korea, April-June  
681 2016), (submitted to AMT), 2018.
- 682 Zhu, Lei, Daniel J. Jacob, Frank N. Keutsch, Loretta J. Mickley, Richard Scheffe, Madeleine Strum, Gonzalo  
683 González Abad, Kelly Chance, Kai Yang, Bernhard Rappenglück, Dylan B. Millet, Munkhbayar Baasandorj,  
684 Lyatt Jaeglé, and Viral Shah, Formaldehyde (HCHO) As a Hazardous Air Pollutant: Mapping Surface Air  
685 Concentrations from Satellite and Inferring Cancer Risks in the United States, Environmental Science &  
686 Technology 51 (10), 5650-5657, DOI: 10.1021/acs.est.7b01356, 2017.

687

688

#### 689 Acknowledgement

690 The author would like to thank the Pandora project for support in completing this study as well  
691 as financial support from the KORUS-AQ project NNH15ZDA001N-KORUS. All data is available from a  
692 NASA data repository: <https://avdc.gsfc.nasa.gov/pub/DSCOVER/Pandora/DATA/KORUS-AQ/>

693

694



695 **Tables**

Table 1 KORUS-AQ Locations (South to North)

| Locations    | Alt(m) | Latitude | Longitude |
|--------------|--------|----------|-----------|
| Gwangju      | 33     | 35.2260N | 126.8430W |
| Busan        | 228    | 35.2353N | 129.0825W |
| Anmyeondo    | 41     | 36.5380N | 126.3300W |
| Taehwa Mtn   | 160    | 37.3123N | 127.3106W |
| Yeoju-1 & 2  | 90     | 37.3385N | 127.4895W |
| Songchon     | 49     | 37.4100N | 127.5600W |
| Olympic Park | 26     | 37.5232N | 127.1260W |
| Seoul        | 181    | 37.5644N | 126.9340W |

696

697

Table 2 Taehwa Mtn DC8 compared to PSI measurements in Fig. 18

| Date   | LT       | DC8 HCHO DU | PSI HCHO | Percent |
|--------|----------|-------------|----------|---------|
| 11 May | 08:25:19 | 0.4         | 0.6      | 67      |
| 18 May | 08:34:26 | 0.4         | 0.5      | 80      |
| 30 May | 12:05:00 | 0.5         | 0.9      | 56      |
| 10 Jun | 08:22:45 | 1           | 1.16     | 86      |
| 10 Jun | 12:22:53 | 1           | 1.5      | 67      |
| 10 Jun | 15:46:03 | 1           | 1.3      | 77      |

698

699



700 **Figure Captions**

701 **Fig. 1** KORUS-AQ sites for 9 Pandora instruments at 8 sites.

702 **Fig. 2a**  $C(\text{NO}_2)$  amounts from Pandora 27 and 35 in Yeosu, Korea during 3 June 2016 and their difference  
703  $(\text{Pan35} - \text{Pan27}) < 0.05$  DU. An estimate of the cloud cover effect on measured radiances  
704 (counts/second) is shown in Fig. 2b.

705 **Fig. 2b** Pandora 35 estimate of cloud or aerosol cover from measured counts/second at approximately  
706 500 nm showing a near noon count rate of  $1.26 \times 10^7$  counts/second followed by a reduced count rate  
707 as clouds move in front of the sun. The cloud or aerosol cover estimate is from the same date 3 June  
708 2016 as the  $C(\text{NO}_2)$  amounts shown in Fig.2a.

709 Fig. 3. Frequency distributions of  $C(\text{NO}_2)$  across the KORUS-AQ PSI network: April 20 to Jun 6 2016,  
710 except as labelled. The axes vary for different sites.

711 Fig. 4  $\text{NO}_2$  time series vs day of the year (DOY) and diurnal variability (daily vertical extent) at 9 Pandora  
712 sites. Notice the very high  $\text{NO}_2$  amounts in Seoul and nearby Olympic Park. The black curves are  
713 approximately weekly least squares running averages. Note: the vertical scales are different for each site  
714 to show the daily variability relative to the running average.

715 Fig. 5  $\text{NO}_2$  amounts vs Day of the Year (DOY) and Local Time for six sites as labeled in each panel. Day  
716 120=April 29, Day 130=May 9, Day 140=May 19, Day 150=May 29, Day 160=June 8, Day 170 =June18.

717 Fig. 6 Approximately 1 year of daily column  $C(\text{NO}_2)$  amount data, the monthly running average amount,  
718 and a linear least squares fit to the deseasonalized time series. The data are from GIST at Gwangju and  
719 Amnyeondo. Panels A and D are the original time series with one data point every 80 seconds, panels B  
720 and E are the deseasonalized time series and the trend in  $C(\text{NO}_2)$ , and panels C and F are monthly  
721 running averages of  $C(\text{NO}_2)$  from the solid lines in panels A and D. The vertical extent (panels A, B, D, and  
722 E) on a given day is the range of diurnal variation from early morning to late afternoon.

723 Fig. 7 (A)  $\text{NO}_2$  time series at Yonsei University in Seoul  $\text{NO}_2$ (grey) and (B) deseasonalized time series.  
724 Combined slope =  $-0.05 \pm 0.001$  DU/Year and Mean =  $1.2 \pm 0.8$  DU or the decrease is  $-4 \pm 0.08$  % / Year.  
725 Seoul has no clear seasonal cycle.

726 Fig. 8 (A) Pusan University in Busan  $\text{NO}_2$  daily time series (grey) and (B) deseasonalized time series with  
727 linear trends.

728 Fig. 9 Comparisons between the daily values of  $C(\text{NO}_2)$  for OMI (black) and PSI (red) at Seoul and Busan  
729 for a 5-year period. Solid lines show the average seasonal variation (Lowess(0.1)), see also Fig. 9b.

730 Fig. 10  $C(\text{NO}_2)$  time series from Pandora (red) and OMI (black) for GIST University in Gwangju Korea and  
731 their differences. The comparison is formed from time coincidences between Pandora and OMI.

732 Fig. 11 A correlation plot of  $C(\text{NO}_2)$  from 4STAR onboard the DC-8 compared to the  $C(\text{NO}_2)$  amount  
733 measured by the PSI at Olympic Park on nine different days. The solid black line is the 1:1 line drawn for



734 reference. The dashed line represents the data linear fit, with a slope of 1.05, and a correlation  
735 coefficient  $r^2 = 0.7$ , as shown on the plot.

736 Fig. 12 C(HCHO) from PSI at Olympic Park for 6 days in June 2016. C(HCHO) on 2 June 2016 has a peak  
737 value of 2.3 DU at 14:30 hours.

738 Fig. 13 Pandora measured formaldehyde amounts vs day of the year and local time for 29 April 2016 to  
739 11 June 2016 in Olympic Park.

740 Fig. 14 HCHO altitude profile measured onboard the DC8 on 4 May at 07:54 (A) and 11:54 (B) local time  
741 over Olympic Park, Korea. Panel C: PSI measurements of total column HCHO. Vertical bars mark the DC8  
742 flight duration for the profiles yielding altitude integrated column amounts of 0.38 and 0.26 DU.

743 Fig. 15 DC-8 HCHO measurements over Olympic Park on June 4. The continuous blue profiles  
744 show the 1-second HCHO data while the black points with error bars show the 10-second  
745 average and standard deviation of this data at points of closest approach above the Olympic  
746 Park site.

747 Fig. 16 HCHO altitude profile measured onboard the DC8 on 5 June at 8:30 (A) and 15:21 (B) local time  
748 over Olympic Park, Korea. Panel C: PSI measurements of total column HCHO. Vertical bars mark the DC8  
749 flight duration for the profiles yielding column amounts of 0.60 and 0.82 DU.

750 Fig. 17 Total column HCHO from Pandora Yonsei University, Seoul for 6 days in June 2016. HCHO on 2  
751 June 2016 has a peak value of 1.2 DU at 13:30 hours.

752 Fig. 18 Total column HCHO from Pandora Taehwa Mountain for 6 days in June 2016. HCHO on 2 June  
753 2016 has a peak value of 1.2 DU at 12:45.

754 Fig. 19a Summary of total column HCHO for the stated dates during the KORUS-AQ campaign. The solid  
755 line is a Lowess(0.1) fit to the data. The sharp cutoffs in panel A, B, and C were caused obstructions of  
756 the direct sun from the PSI FOV in the afternoon.

757 Fig. 19b Summary of total column HCHO for the stated dates during the KORUS-AQ campaign. Panels A  
758 and B represent the daily variation at a given local time. The solid line is a Lowess(0.1) fit to the data.  
759 Panels C and D show the frequency of occurrence (%) for different amounts of HCHO.

760 Fig. 20 The springtime change in C(HCHO) over about a 40 day period depending on the site.  
761 The “vertical bars” are the diurnal variation within each day of data. The thicker red curve is a  
762 Lowess(0.3) fit to the data, while the thin red line is a linear least squares fit. The Lowess(0.3) fit  
763 is approximately a 10-day local least-squares average.

764 Fig. 21 Compare PSI • and OMI ◦ retrievals of C(HCHO) at  $13.5 \pm 0.5$  hours.

765

766



767 Figures

768

769

770

771

772

773

774

775

776

777

778

779

780

781

782

783

784 **F01**

785



**Fig. 1** KORUS-AQ sites for 9 Pandora instruments at 8 sites.

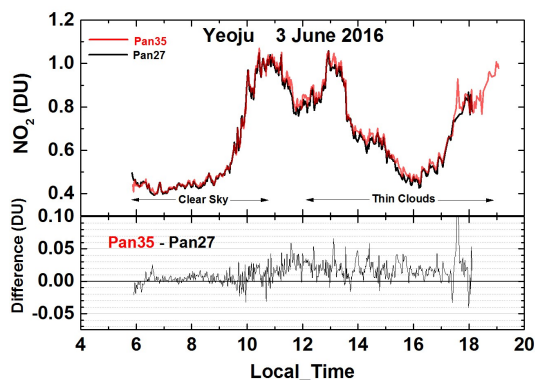


**Fig. 2a**  $C(\text{NO}_2)$  amounts from Pandora 27 and 35 in Yeosu, Korea during 3 June 2016 and their difference ( $\text{Pan35} - \text{Pan27}$ )  $< 0.05$  DU. An estimate of the cloud cover effect on measured radiances (counts/second) is shown in Fig. 2b.

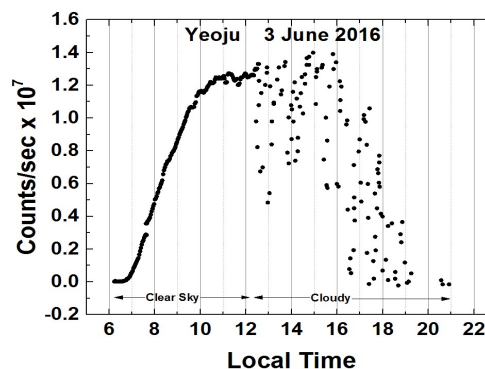


**Fig. 2b** Pandora 35 estimate of cloud or aerosol cover from measured counts/second at approximately 500 nm showing a near noon count rate of  $1.26 \times 10^7$  counts/second followed by a reduced count rate as clouds move in front of the sun. The cloud or aerosol cover estimate is from the same date 3 June 2016 as the  $C(\text{NO}_2)$  amounts shown in Fig. 2a.

786

787 **F02**

788

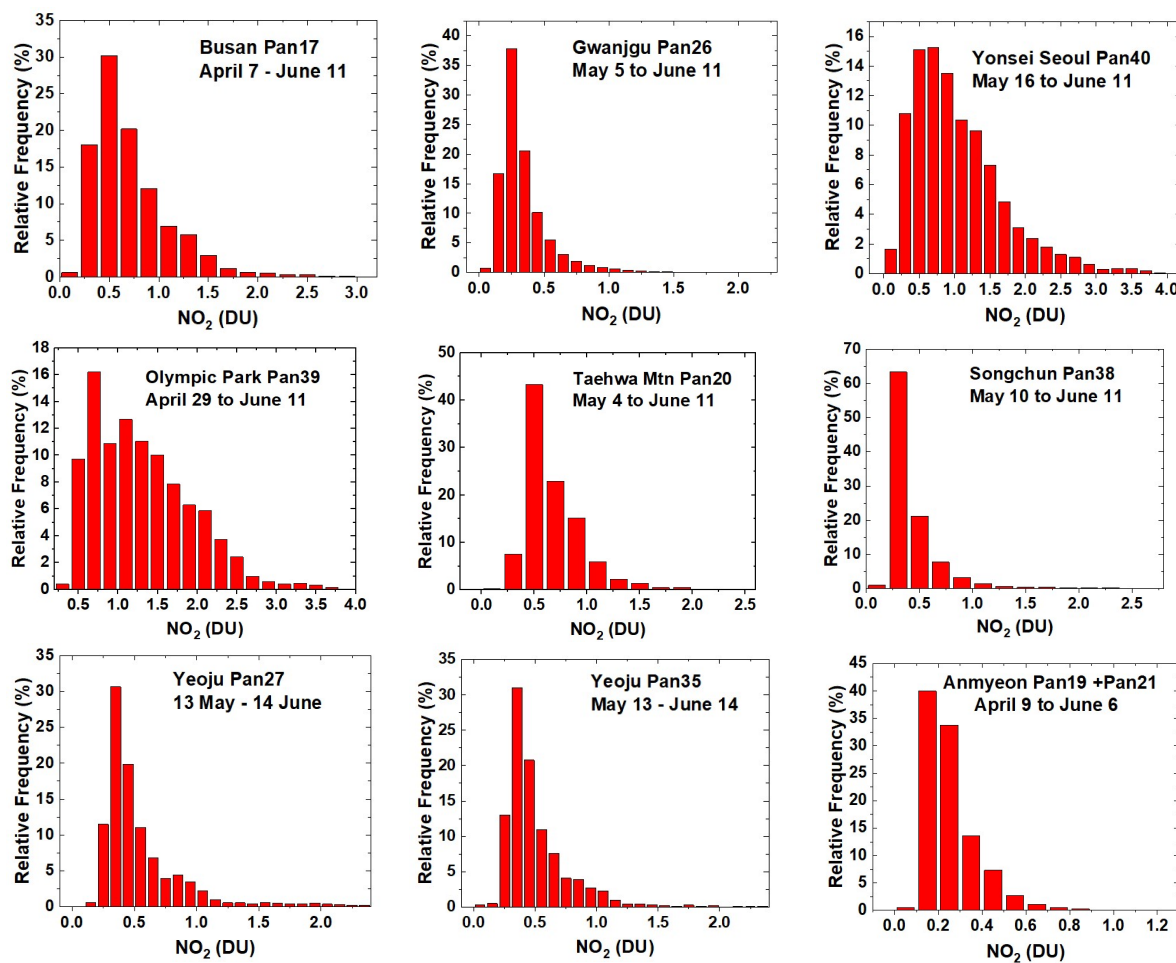


Fig. 3. Frequency distributions of  $C(\text{NO}_2)$  across the KORUS-AQ PSI network: April 20 to Jun 6 2016, except as labelled. The axes vary for different sites.

789

790 **F03**

791

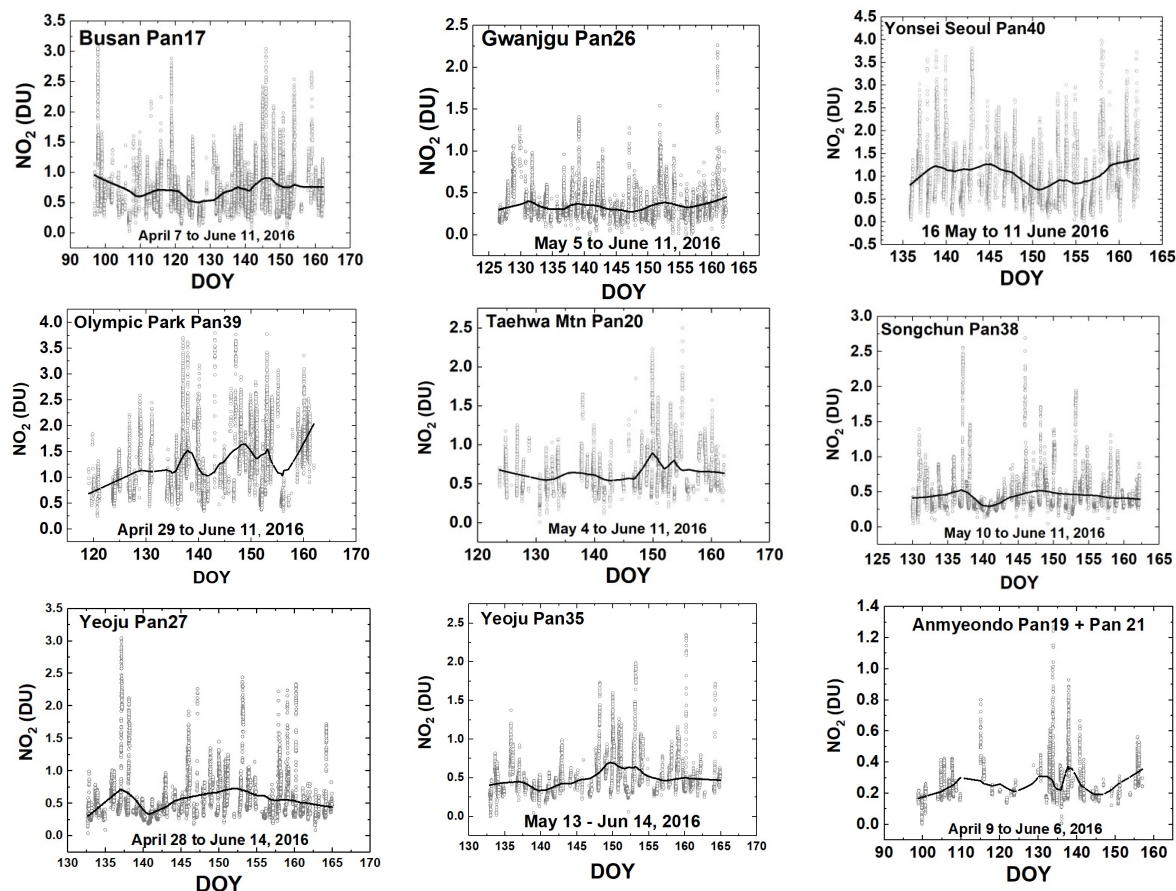


Fig. 4 NO<sub>2</sub> time series vs day of the year (DOY) and diurnal variability (daily vertical extent) at 9 Pandora sites. Notice the very high NO<sub>2</sub> amounts in Seoul and nearby Olympic Park. The black curves are approximately weekly least squares running averages. The daily vertical extent corresponds to diurnal variation (Fig. 2). Note: the vertical scales are different for each site to show the daily variability relative to the running average.

792

793 **F04**

794

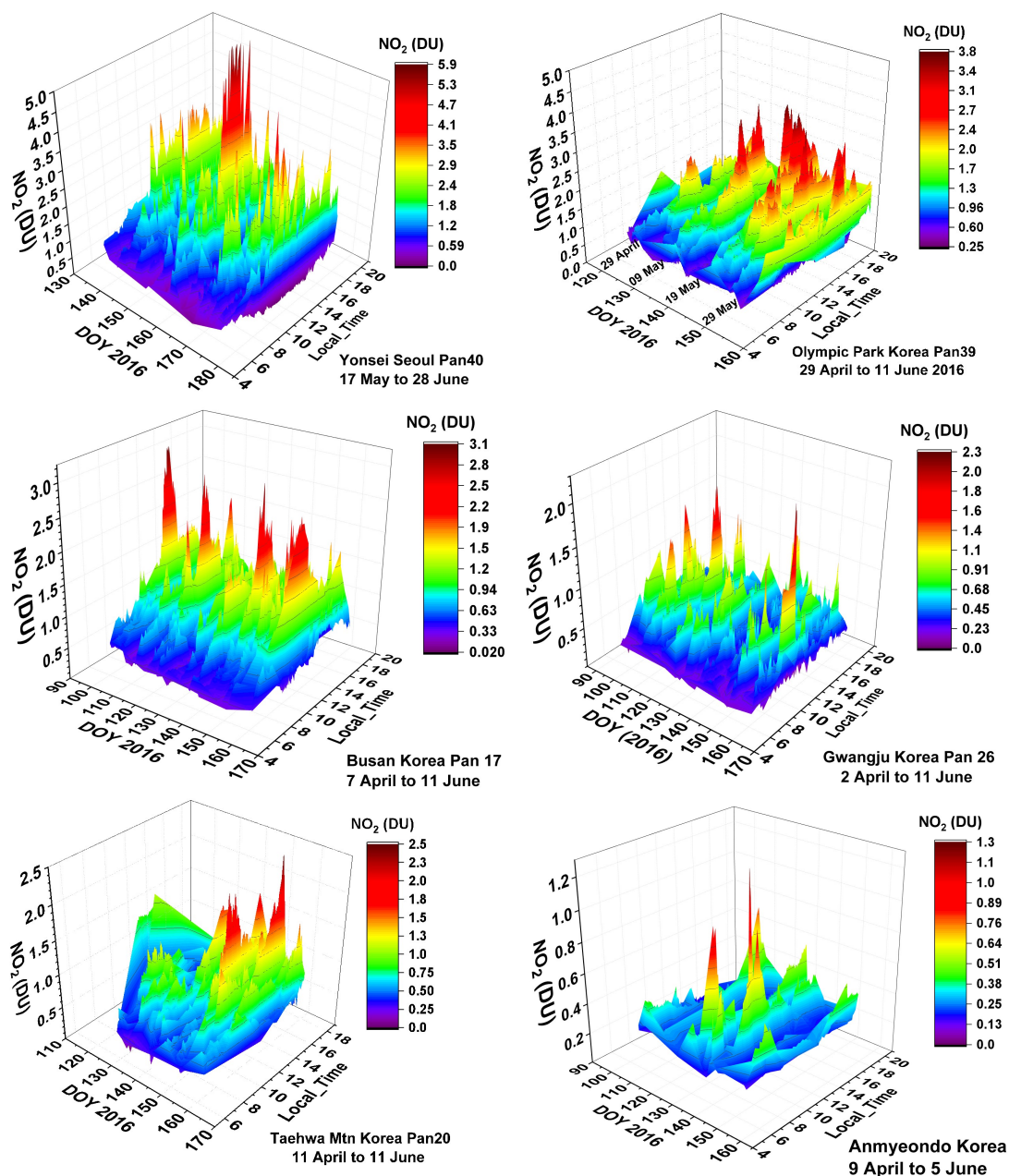


Fig. 5 NO<sub>2</sub> amounts vs Day of the Year (DOY) and Local Time for six sites as labeled in each panel. Day 120=April 29, Day 130=May 9, Day 140=May 19, Day 150=May 29, Day 160=June 8, Day 170 =June18.

795

796 **F05**



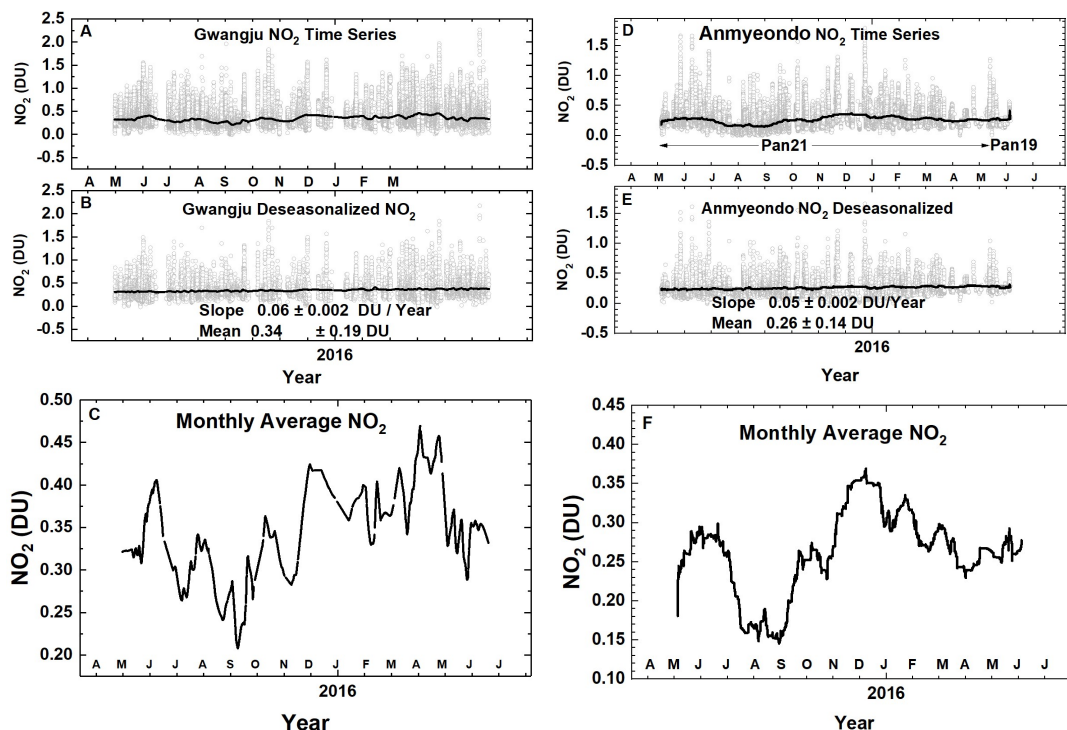


Fig. 6 Approximately 1 year of daily column C(NO<sub>2</sub>) amount data , the monthly running average, and a linear least squares fit to the deseasonalized time series. The data are from GIST at Gwangju and Anmyeondo. Panels A and D are the original time series with one data point every 80 seconds, panels B and E are the deseasonalized time series and the trend in C(NO<sub>2</sub>), and panels C and F are monthly running averages of C(NO<sub>2</sub>) from the solid lines in panels A and D. The vertical extent (panels A, B, D, and E) on a given day is the range of diurnal variation from early morning to late afternoon.

798

799 **F06**

800

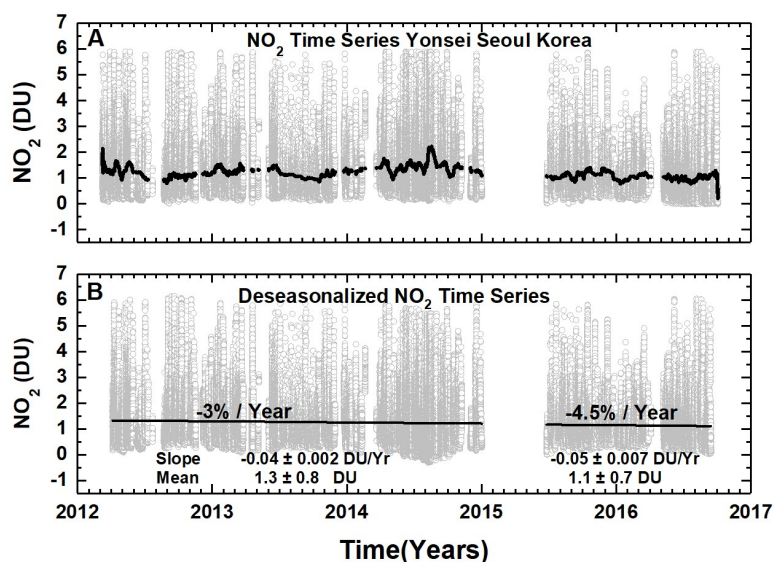


Fig. 7 (A) NO<sub>2</sub> time series at Yonsei University in Seoul NO<sub>2</sub>(grey) and (B) deseasonalized time series. Combined slope =  $-0.05 \pm 0.001$  DU/Year and Mean =  $1.2 \pm 0.8$  DU or the decrease is  $-4 \pm 0.08$  % / Year. Seoul has no clear seasonal cycle.

801

802 **F07**

803

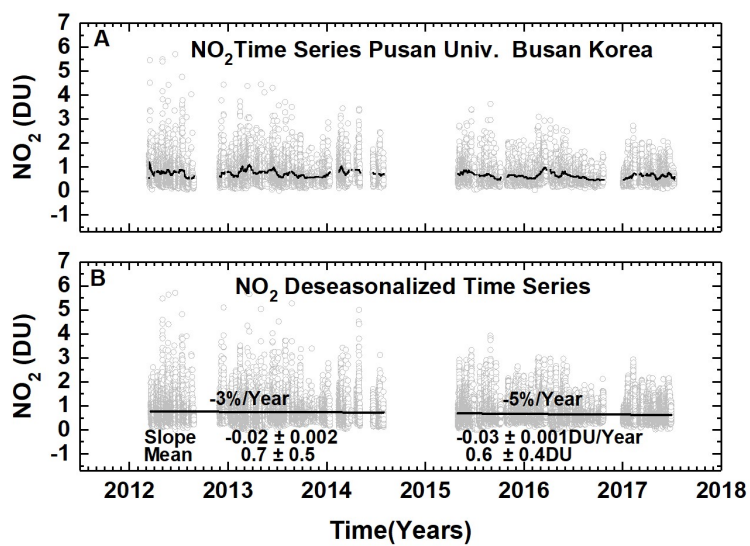


Fig. 8 (A) Pusan University in Busan NO<sub>2</sub> daily time series (grey) and (B) deseasonalized time series with linear trends.

804

805 **F08**

806

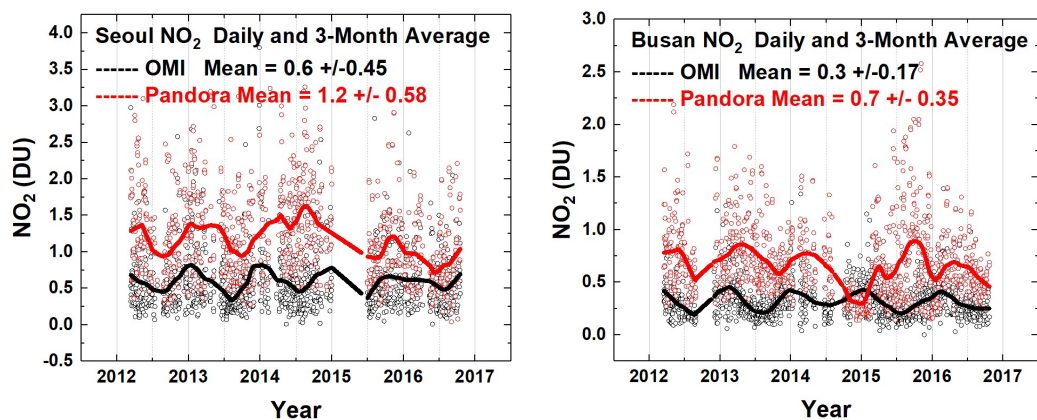


Fig. 9a Comparisons between the daily values of C(NO<sub>2</sub>) for OMI (black) and PSI (red) at Seoul and Busan for a 5-year period. Solid lines show the average seasonal variation (Lowess(0.1)), see also Fig. 9b.

807

808 **F09**

809

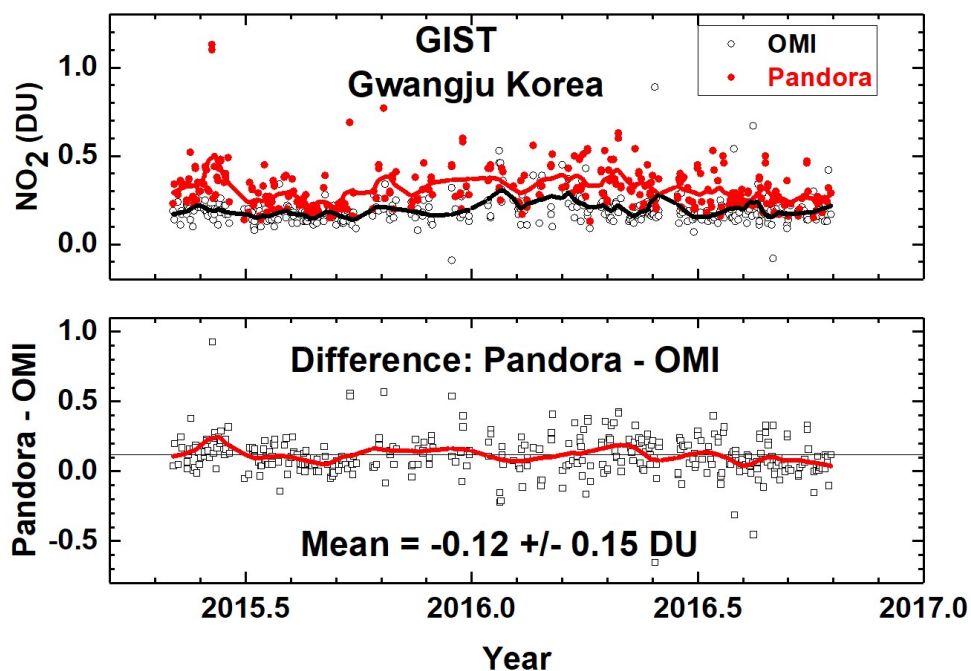


Fig. 10 C(NO<sub>2</sub>) time series from Pandora (red) and OMI (black) for GIST University in Gwangju Korea and their differences. The comparison is formed from time coincidences between Pandora and OMI.

810

811 **F10**

812

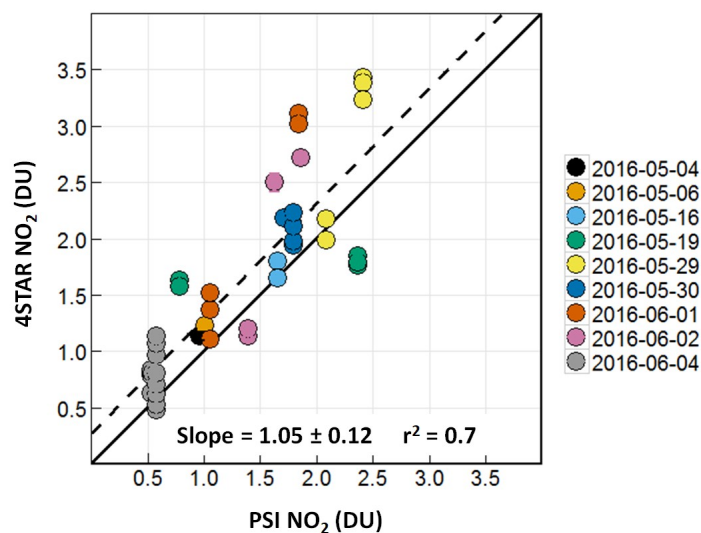


Fig. 11 A correlation plot of C(NO<sub>2</sub>) from 4STAR onboard the DC-8 compared to the C(NO<sub>2</sub>) amount measured by the PSI at Olympic Park on nine different days. The solid black line is the 1:1 line drawn for reference. The dashed line represents the data linear fit, with a slope of 1.05, and a correlation coefficient  $r^2 = 0.7$ , as shown on the plot.

813

814 **F11**

815

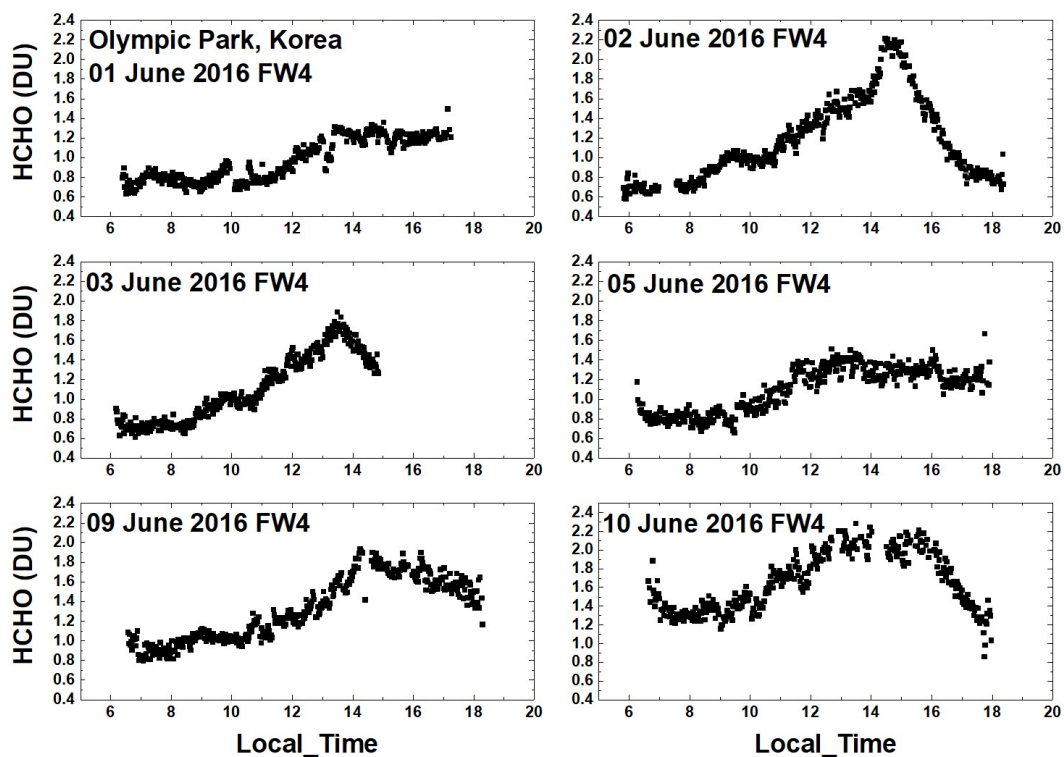


Fig. 12 C(HCHO) from PSI at Olympic Park for 6 days in June 2016. C(HCHO) on 2 June 2016 has a peak value of 2.3 DU at 14:30 hours.

816

817 **F12**

818

819

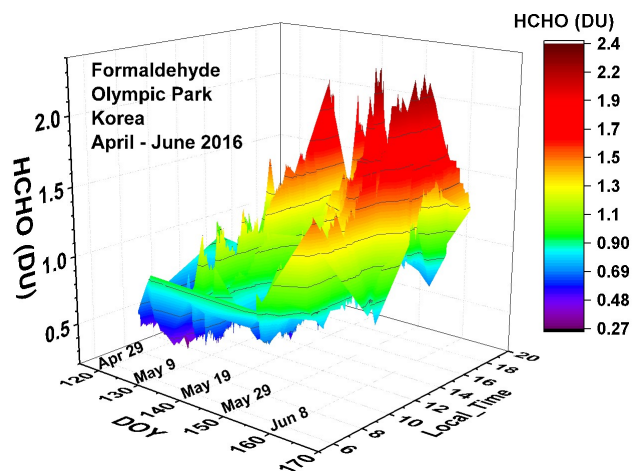


Fig. 13 Pandora measured formaldehyde amounts vs day of the year and local time for 29 April 2016 to 11 June 2016 in Olympic Park.

820

821 **F13**

822

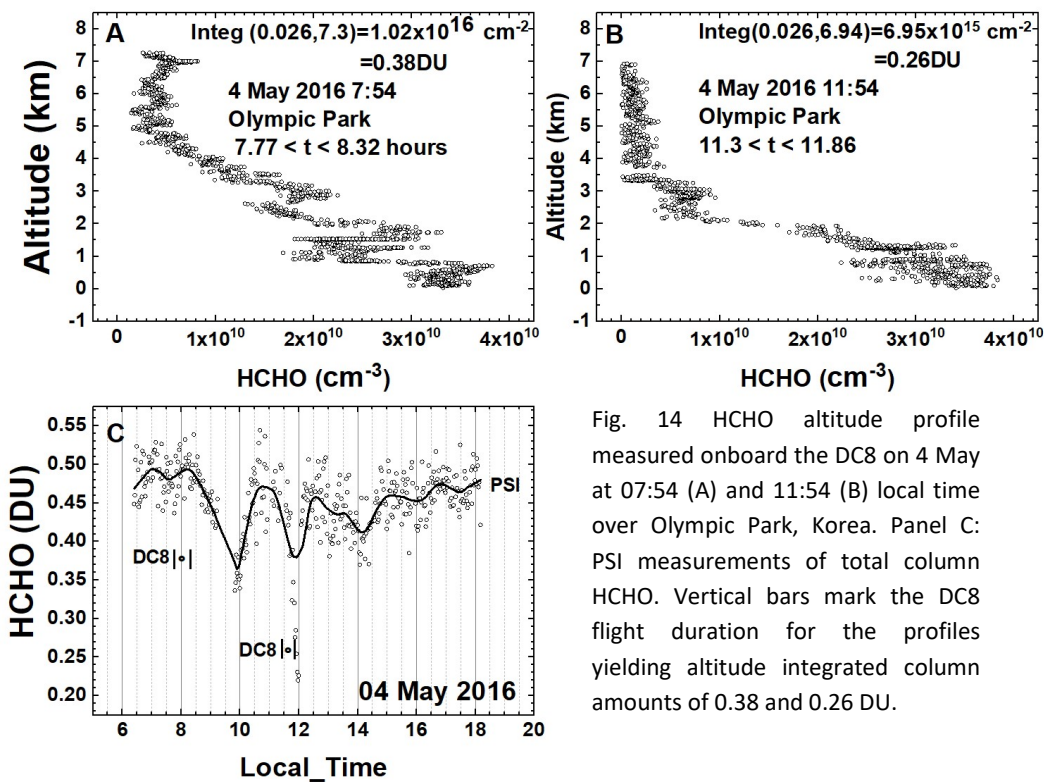


Fig. 14 HCHO altitude profile measured onboard the DC8 on 4 May at 07:54 (A) and 11:54 (B) local time over Olympic Park, Korea. Panel C: PSI measurements of total column HCHO. Vertical bars mark the DC8 flight duration for the profiles yielding altitude integrated column amounts of 0.38 and 0.26 DU.

823

824 **F14**

825

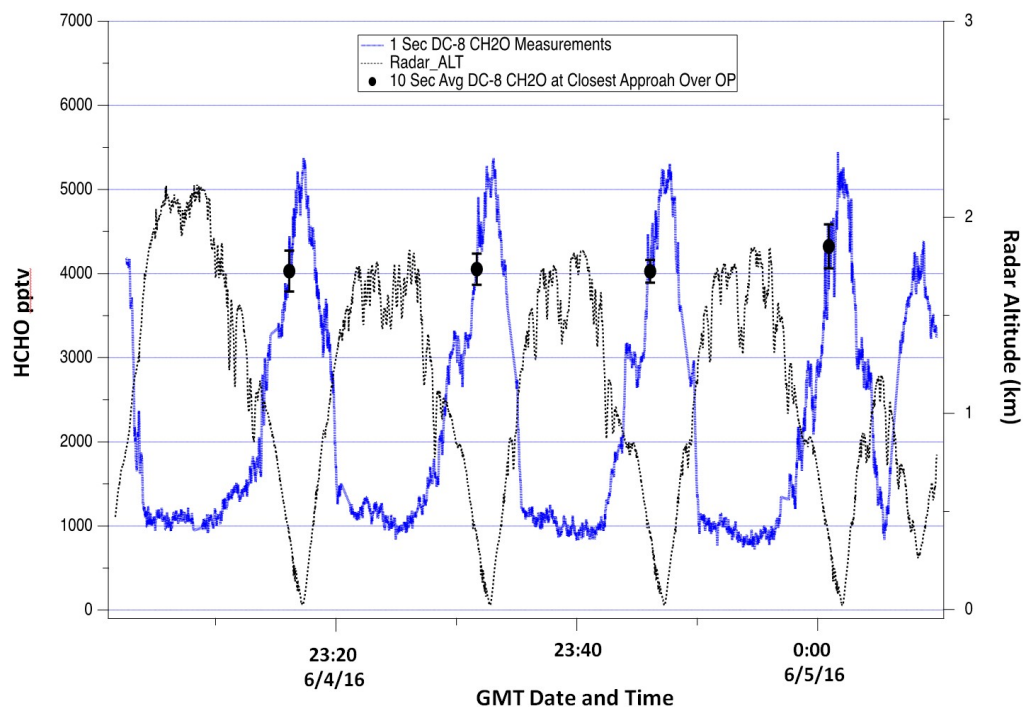


Fig. 15 DC-8 HCHO measurements over Olympic Park on June 4. The continuous blue profiles show the 1-second HCHO data while the black points with error bars show the 10-second average and standard deviation of this data at points of closest approach above the Olympic Park site.

826

827 **F15**

828

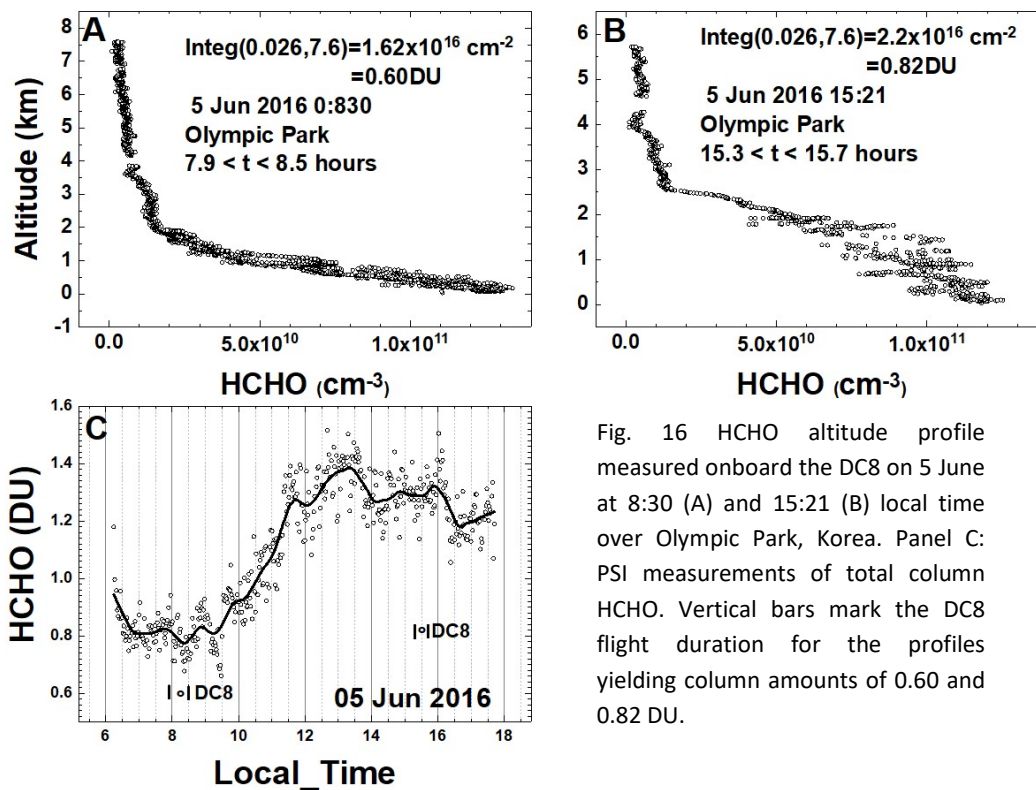


Fig. 16 HCHO altitude profile measured onboard the DC8 on 5 June at 8:30 (A) and 15:21 (B) local time over Olympic Park, Korea. Panel C: PSI measurements of total column HCHO. Vertical bars mark the DC8 flight duration for the profiles yielding column amounts of 0.60 and 0.82 DU.

829

830 **F16**

831

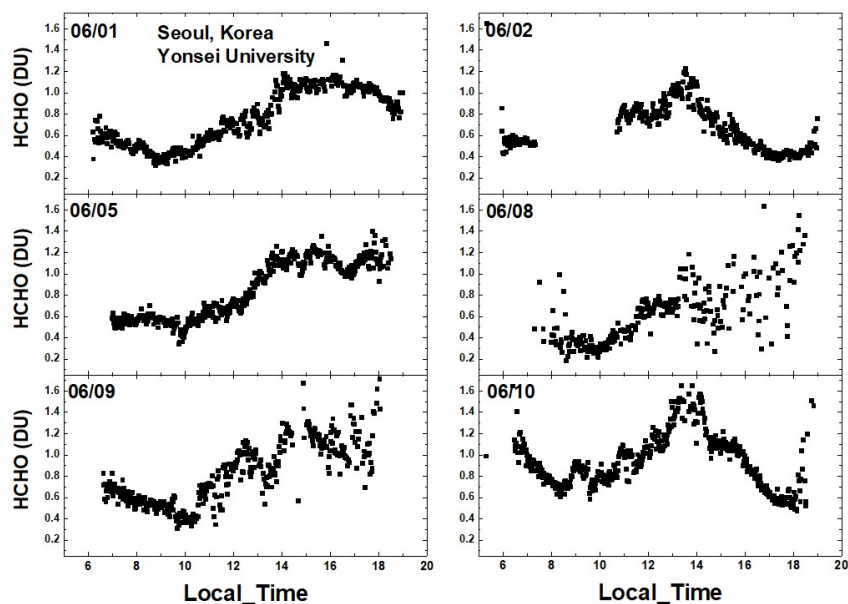


Fig. 17 Total column HCHO from Pandora Yonsei University, Seoul for 6 days in June 2016. HCHO on 2 June 2016 has a peak value of 1.2 DU at 13:30 hours.

832

833 **F17**

834

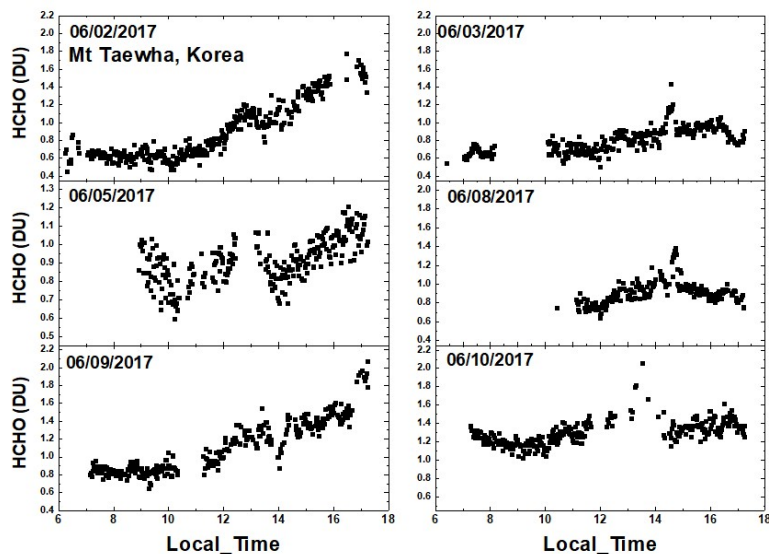


Fig. 18 Total column HCHO from Pandora Taehwa Mountain for 6 days in June 2016. HCHO on 2 June 2016 has a peak value of 1.2 DU at 12:45.

835

836 **F18**

837

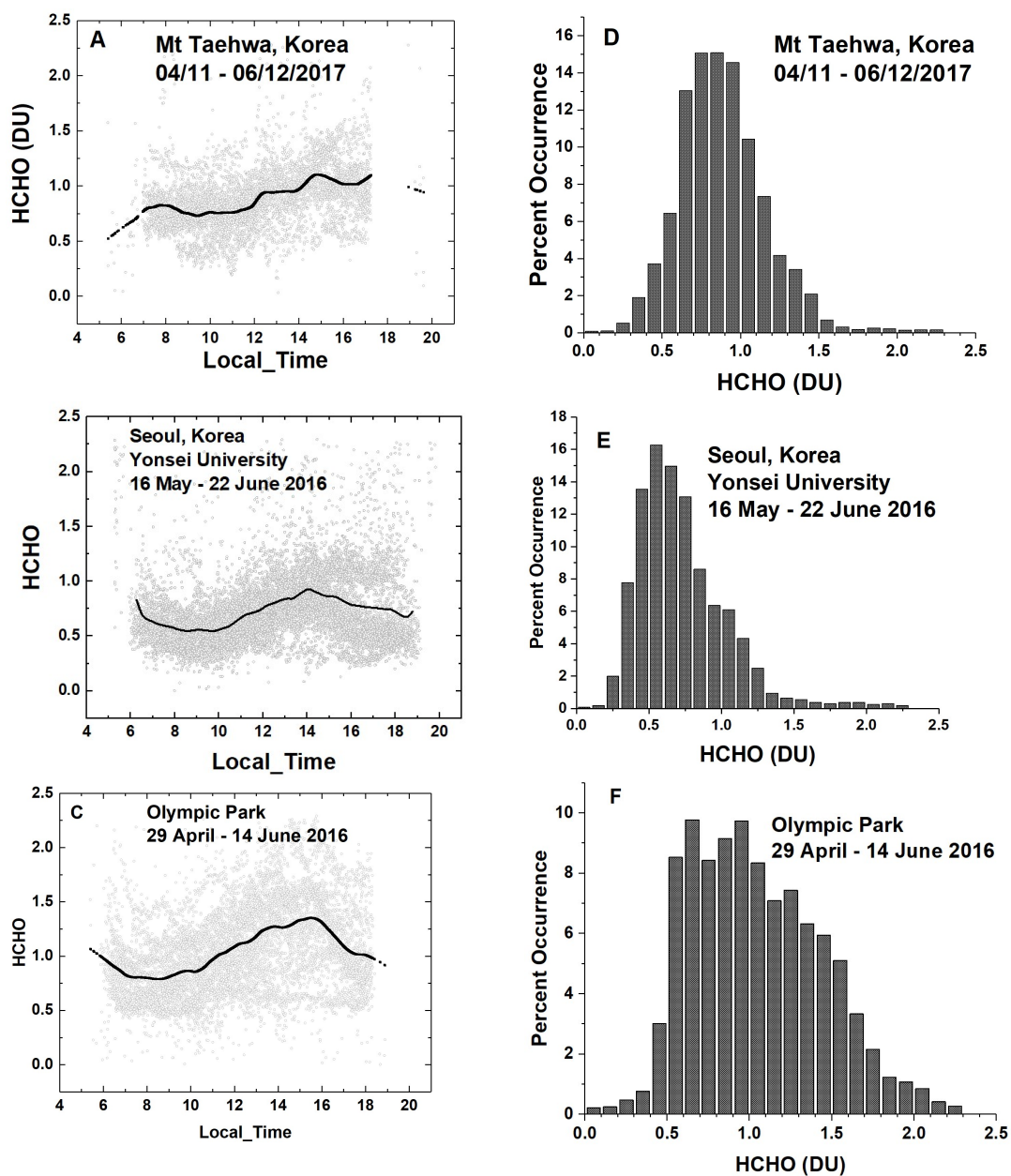


Fig. 19a Summary of total column HCHO for the stated dates during the KORUS-AQ campaign. The solid line is a Lowess(0.1) fit to the data. The sharp cutoffs in panel A, B, and C were caused obstructions of the direct sun from the PSI FOV in the afternoon.

838

839 **F19a**



840

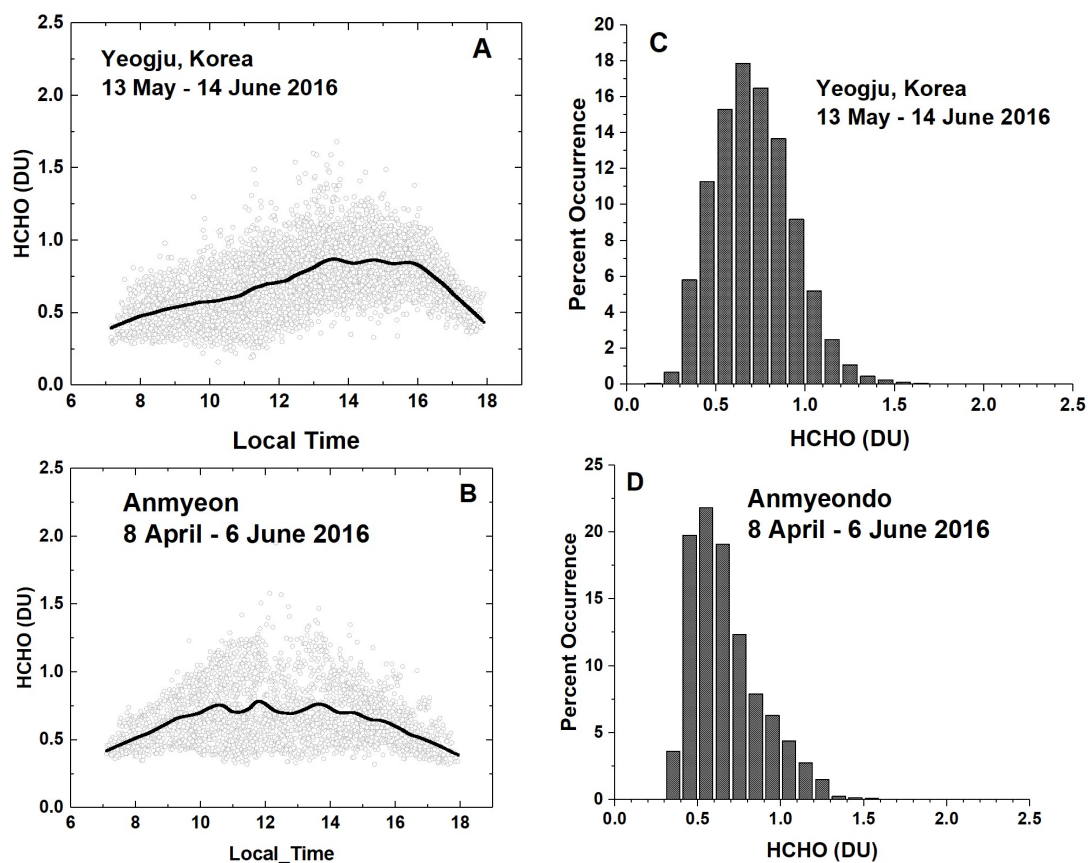


Fig. 19b Summary of total column HCHO for the stated dates during the KORUS-AQ campaign. Panels A and B represent the daily variation at a given local time. The solid line is a Lowess(0.1) fit to the data. Panels C and D show the frequency of occurrence (%) for different amounts of HCHO.

841

842 **F19b**

843



844

845

846

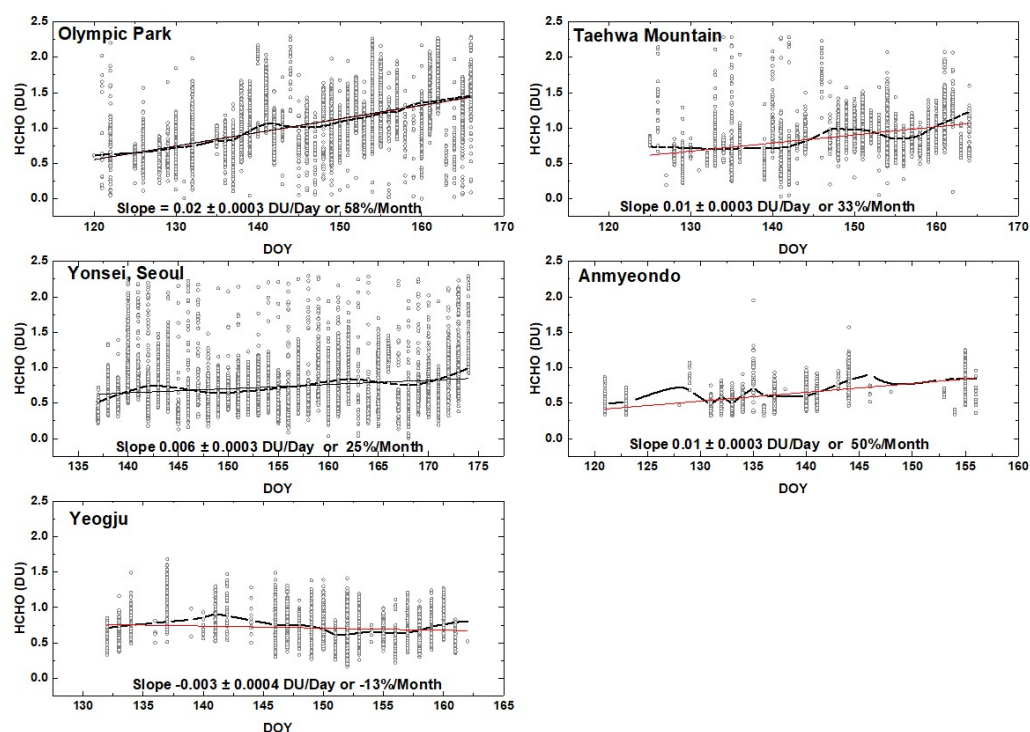


Fig. 20 The springtime change in C(HCHO) over about a 40 day period depending on the site. The “vertical bars” are the diurnal variation within each day of data. The thicker red curve is a Lowess(0.3) fit to the data, while the thin red line is a linear least squares fit. The Lowess(0.3) fit is approximately a 10-day local least-squares average.

847

848 **F20**

849

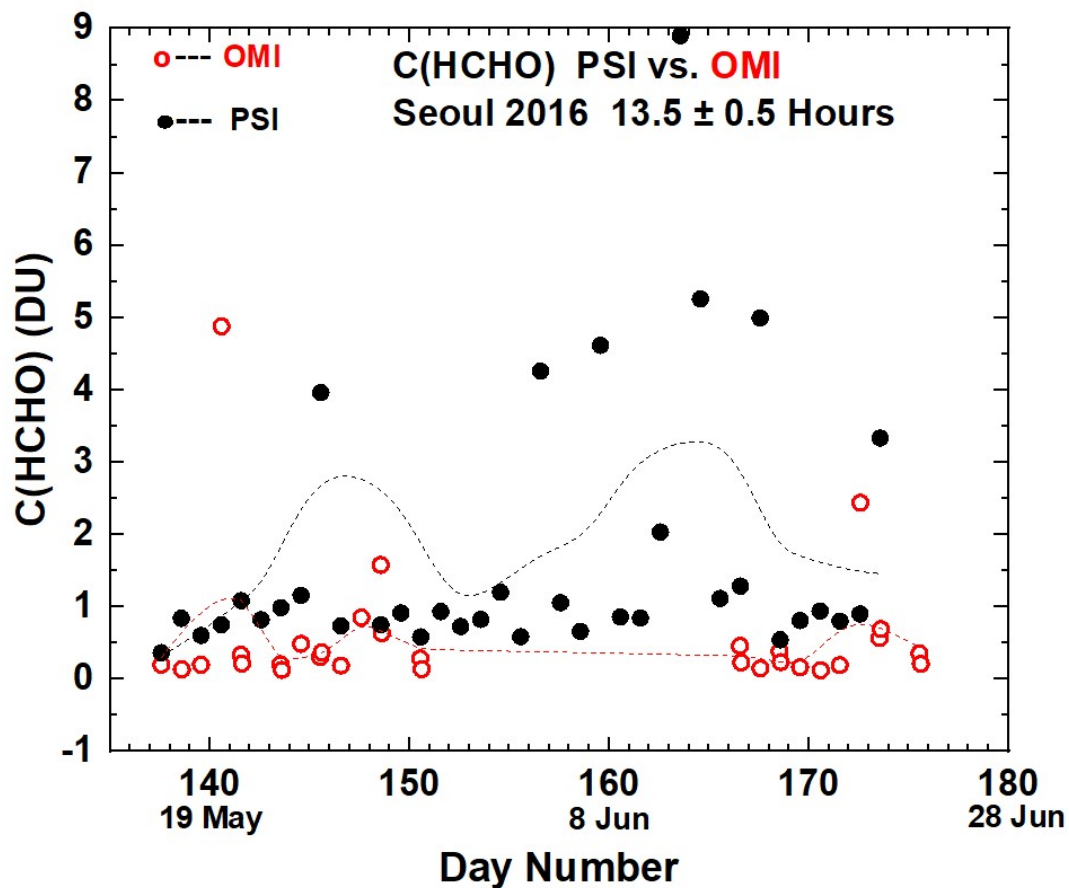


Fig. 21 Compare PSI • and OMI ◯ retrievals of C(HCHO) at 13.5 ± 0.5 hours.

850

851 **F21**